*Published in : Science Immunology (2024), vol. 9, eadk3981*
*DOI: 10.1126/sciimmunol.adk3981*
*Status : Postprint (Author's version)*

# TIMING AND LOCATION DICTATE MONOCYTE FATE AND THEIR TRANSITION TO TUMOR- ASSOCIATED MACROPHAGES

Garett Dunsmore

*Institut Gustave Roussy, INSERM U1015, Bâtiment de Médecine Moléculaire 114, rue Edouard Vaillant, 94800 Villejuif, France – Université Paris-Saclay, Ile-de-France, France.*

Wei Guo

*Shanghai Institute of Immunology, Department of Immunology and Microbiology, Shanghai Jiao Tong University School of Medicine, Shanghai 200025, China.*

Ziyi Li

*Shanghai Institute of Immunology, Department of Immunology and Microbiology, Shanghai Jiao Tong University School of Medicine, Shanghai 200025, China.*

David Alejandro Bejarano

*Quantitative Systems Biology, Life and Medical Sciences Institute, University of Bonn, 53115 Bonn, Germany.*

Rhea Pai

*Curtin Medical School, Curtin University, Bentley, WA, Australia.*

Katharine Yan

*Singapore Immunology Network (SIgN), A*STA R, 8A Biomedical Grove, Immunos Building, Level 3, Singapore 138648, Singapore.*

Immanuel Kwok

*Singapore Immunology Network (SIgN), A*STA R, 8A Biomedical Grove, Immunos Building, Level 3, Singapore 138648, Singapore.*

Leonard Tan

*Singapore Immunology Network (SIgN), A*STA R, 8A Biomedical Grove, Immunos Building, Level 3, Singapore 138648, Singapore.*

Melissa Ng

*Singapore Immunology Network (SIgN), A*STA R, 8A Biomedical Grove, Immunos Building, Level 3, Singapore 138648, Singapore.*

*Published in : Science Immunology (2024), vol. 9, eadk3981*
*DOI: 10.1126/sciimmunol.adk3981*
*Status : Postprint (Author's version)*

Carlos De La Calle Fabregat

*Institut Gustave Roussy, INSERM U1015, Bâtiment de Médecine Moléculaire 114, rue Edouard Vaillant, 94800 Villejuif, France.*

Aline Yatim

*Institut Curie, PSL University, INSERM U932, Immunity and Cancer, 75005 Paris, France.*

Antoine Bougouin

*Centre de Recherche des Cordeliers, INSERM, Sorbonne Université, USPC Université Paris Cité, Equipe Labellisée Ligue Nationale Contre le Cancer, Paris, France.*

Kevin Mulder

*Institut Gustave Roussy, INSERM U1015, Bâtiment de Médecine Moléculaire 114, rue Edouard Vaillant, 94800 Villejuif, France – Université Paris-Saclay, Ile-de-France, France.*

Jake Thomas

Quantitative Systems Biology, Life and Medical Sciences Institute, University of Bonn, 53115 Bonn, Germany.

Javiera Villar

*Institut Gustave Roussy, INSERM U1015, Bâtiment de Médecine Moléculaire 114, rue Edouard Vaillant, 94800 Villejuif, France.*

Mathilde Bied

*Institut Gustave Roussy, INSERM U1015, Bâtiment de Médecine Moléculaire 114, rue Edouard Vaillant, 94800 Villejuif, France – Université Paris-Saclay, Ile-de-France, France.*

Benoit Kloeckner

*Institut Gustave Roussy, INSERM U1015, Bâtiment de Médecine Moléculaire 114, rue Edouard Vaillant, 94800 Villejuif, France – Université Paris-Saclay, Ile-de-France, France.*

Charles-Antoine Dutertre

*Institut Gustave Roussy, INSERM U1015, Bâtiment de Médecine Moléculaire 114, rue Edouard Vaillant, 94800 Villejuif, France.*

Grégoire Gessain

*Institut Gustave Roussy, INSERM U1015, Bâtiment de Médecine Moléculaire 114, rue Edouard Vaillant, 94800 Villejuif, France.*

Svetoslav Chakarov

*Shanghai Institute of Immunology, Department of Immunology and Microbiology, Shanghai Jiao Tong University School of Medicine, Shanghai 200025, China.*

*Published in : Science Immunology (2024), vol. 9, eadk3981*
*DOI: 10.1126/sciimmunol.adk3981*
*Status : Postprint (Author's version)*

Zhaoyuan Liu

*Shanghai Institute of Immunology, Department of Immunology and Microbiology, Shanghai Jiao Tong University School of Medicine, Shanghai 200025, China.*

Jean-Yves Scoazec

*Institut Gustave Roussy, INSERM U1015, Bâtiment de Médecine Moléculaire 114, rue Edouard Vaillant, 94800 Villejuif, France.*

Ana-Maria Lennon- Dumenil

*Institut Curie, PSL University, INSERM U932, Immunity and Cancer, 75005 Paris, France.*

Thomas Marichal

*Laboratory of Immunophysiology, GIGA Institute, Liège University, Liège, Belgium – Faculty of Veterinary Medicine, Liège University, Liège, Belgium – Walloon Excellence in Life Sciences and Biotechnology (WELBIO) Department, WEL Research Institute, Wavre, Belgium.*

Catherine Sautès-Fridman

*Centre de Recherche des Cordeliers, INSERM, Sorbonne Université, USPC Université Paris Cité, Equipe Labellisée Ligue Nationale Contre le Cancer, Paris, France.*

Wolf Herman Fridman

*Centre de Recherche des Cordeliers, INSERM, Sorbonne Université, USPC Université Paris Cité, Equipe Labellisée Ligue Nationale Contre le Cancer, Paris, France.*

Ankur Sharma

*Curtin Medical School, Curtin University, Bentley, WA, Australia – Harry Perkins Institute of Medical Research, QEII Medical Centre and Centre for Medical Research, 6 Verdun Street, Nedlands, Perth, WA 6009, Australia – Institute of Molecular and Cellular Biology, A*STA R, Singapore 138673, Singapore – KK Research Centre, KK Women's and Children's Hospital, Singapore 229899, Singapore – Translational Genomics Program, Garvan Institute of Medical Research and Kinghorn Cancer Centre, Darlinghurst, NSW, Australia.*

Bing Su

*Shanghai Institute of Immunology, Department of Immunology and Microbiology, Shanghai Jiao Tong University School of Medicine, Shanghai 200025, China.*

Andreas Schlitzer

*Quantitative Systems Biology, Life and Medical Sciences Institute, University of Bonn, 53115 Bonn, Germany.*

Lai Guan Ng*

*Shanghai Immune Therapy Institute Renji Hospital, Shanghai Jiao Tong University School of Medicine, Shanghai 200010, China – Department of Microbiology and Immunology, National University of Singapore, Singapore, Singapore.*

*Published in : Science Immunology (2024), vol. 9, eadk3981*
*DOI: 10.1126/sciimmunol.adk3981*
*Status : Postprint (Author's version)*

Camille Blériot*

*Institut Gustave Roussy, INSERM U1015, Bâtiment de Médecine Moléculaire 114, rue Edouard Vaillant, 94800 Villejuif, France – Institut Necker Enfants Malades (INEM), CNRS UMR 8253, INSERM U1151, 160 rue de Vaugirard, 75015 Paris, France.*

Florent Ginhoux*

*Institut Gustave Roussy, INSERM U1015, Bâtiment de Médecine Moléculaire 114, rue Edouard Vaillant, 94800 Villejuif, France – Université Paris-Saclay, Ile-de-France, France – Shanghai Institute of Immunology, Department of Immunology and Microbiology, Shanghai Jiao Tong University School of Medicine, Shanghai 200025, China – Singapore Immunology Network (SIgN), A*STA R, 8A Biomedical Grove, Immunos Building, Level 3, Singapore 138648, Singapore – Department of Medicine, Yong Loo Lin School of Medicine, National University of Singapore, Singapore 119228 Singapore.*

**Abstract.** Tumor- associated macrophages (TAMs) are a heterogeneous population of cells whose phenotypes and functions are shaped by factors that are incompletely understood. Herein, we asked when and where TAMs arise from blood monocytes and how they evolve during tumor development. We initiated pancreatic ductal adenocarcinoma (PDAC) in inducible monocyte fate- mapping mice and combined single- cell transcriptomics and high- dimensional flow cytometry to profile the monocyte- to- TAM transition. We revealed that monocytes differentiate first into a transient intermediate population of TAMs that generates two longer-lived lineages of terminally differentiated TAMs with distinct gene expression profiles, phenotypes, and intra tumoral localization. Transcriptome datasets and tumor samples from patients with PDAC evidenced parallel TAM populations in humans and their prognostic associations. These insights will support the design of new therapeutic strategies targeting TAMs in PDAC.

# INTRODUCTION

Recent advances in our understanding of the tumor microenvironment (TME), including the roles of immune cells, have led to the development of immunotherapies (*1*, *2*) with tumor-type–specific efficacy. Whereas some immunotherapies such as treatment with anti– programmed cell death protein 1 (PD- 1) antibodies have shown high efficacy in treating melanoma (*3*), immunotherapy has shown very little benefit for patients with pancreatic ductal adenocarcinoma (PDAC) (*4*). A deeper understanding of TME biology, specifically within the immune compartment, is needed to understand these differences.

Tumor- associated macrophages (TAMs) are the most abundant immune cells in the TME, where they support tumor growth, angiogenesis, extracellular matrix remodeling, immune modulation/suppression, and metastatic spread (*5*, *6*). Furthermore, recent single-cell RNA sequencing (scRNA- seq) analyses have identified subpopulations of TAMs that inhabit distinct locations and have various functions within the TME (*7*, *8*). Thus, although TAMs are a promising potential target for future immunotherapies, we do not yet fully understand their developmental trajectories or the spatial relationships between distinct TAM subpopulations.

*Published in : Science Immunology (2024), vol. 9, eadk3981*
*DOI: 10.1126/sciimmunol.adk3981*
*Status : Postprint (Author's version)*

Key factors determining macrophage identity include their ontogeny, their niche of residence, and the homeostatic or inflammatory signals that they encounter (*9*). Macrophages can be derived either from embryonic precursors or adult circulating monocytes, with each tissue inhabited by a characteristic proportion of these two ontogenically distinct macrophage populations (*10*). Such equilibrium is subject to change in the TME, given that studies in a murine model of PDAC revealed that ~70% of TAMs were of monocytic origin and exhibited different functional profiles compared with embryonically derived TAMs (*11*). Furthermore, differential localization between embryonically derived and monocyte- derived TAMs according to their origin was recently observed in murine and human non–small cell lung carcinoma (*12*). In addition, residency duration is another newly identified parameter shaping macrophage identity (*9*). Gradually, a picture of the dynamic environment of tumors, which both is reciprocally shaped by and shapes TAM diversity, is emerging.

Here, we aimed to refine our understanding of the dynamic monocyte- to- TAM transition in PDAC and to define the developmental relationships between TAM subpopulations. We exploited PDAC-bearing monocyte fate- mapping and inducible Cre recombinase fused to a mutant estrogen ligand-binding domain (CreERT2) monocyte fate- mapping (time- stamping) mouse models that enabled us to track monocytes within the TME. Using this approach, we identified a pathway linking monocytes to specific TAM subpopulations with distinct localization and functional profiles, with relevant parallels in human PDAC.

# RESULTS

### Origin of TAMs in a murine model of PDAC

To quantify the relative contribution of embryonic precursors and circulating monocytes to the TAM pool in PDAC, we used *Ms4a3*$^{Cre}$ x *Rosa*$^{tdTomato}$ mice, in which all granulocyte- monocyte progenitor (GMP)–derived circulating monocytes and their progeny are stably fluorescently tagged, whereas embryonically derived macrophages are not (*13*). We injected *Pdx1*$^{Cre}$ *LSL-Kras* $^{G12D}$ *LSL-Tp53* $^{R172H}$ (KPC) cells orthotopically into the pancreases of these mice and conducted scRNA- seq on the immune cells (CD45$^+$) isolated from tumors after 35 days (Fig. 1A). We then measured expression of canonical marker genes to cluster and annotate the immune cell populations present (fig. S1, A and B, and data file S1). As expected, tdTomato was expressed by all neutrophils, some mononuclear phagocytes, but not by T, B, or plasma cell clusters (fig. S1, C and D) (*13*). Within the cluster of mononuclear phagocytes, we identified three populations of cells: tdTomato$^+$ monocytes (expressing *Ly6c2*, *Hp*, *S100a4*, and *Plac8*); macrophages (expressing *Pf4*, *C1qa*, *C1qc*, and *Arg1*), of which around 90% were tdTomato$^+$; and dendritic cells (DCs; expressing *Clec10a*, *H2- Aa*, *H2- Dmb2*, and *Ckb*), among which ~10% were tdTomato$^+$ (Fig. 1, B to E; fig. S1E; and data file S2). Focusing on macrophages, we observed that tdTomato$^-$ cells (embryonically derived) expressed genes specific to resident tissue macrophages (RTMs) [*Folr2* and *Timd4*, for example; (*14*, *15*)], whereas tdTomato$^+$ macrophages (GMP- derived) exhibited a more inflammatory phenotype (expressing *Il1b* and *Il6*) (Fig. 1F and data file S3). Gene ontology (GO) analysis showed that embryonic TAMs expressed genes that were associated with

*Published in : Science Immunology (2024), vol. 9, eadk3981*
*DOI: 10.1126/sciimmunol.adk3981*
*Status : Postprint (Author's version)*

extracellular matrix remodeling, whereas monocyte-derived TAMs exhibited proinflammatory expression patterns (Fig. 1G), consistent with previous work on murine PDAC (*11*).

## MONOCYTE- DERIVED

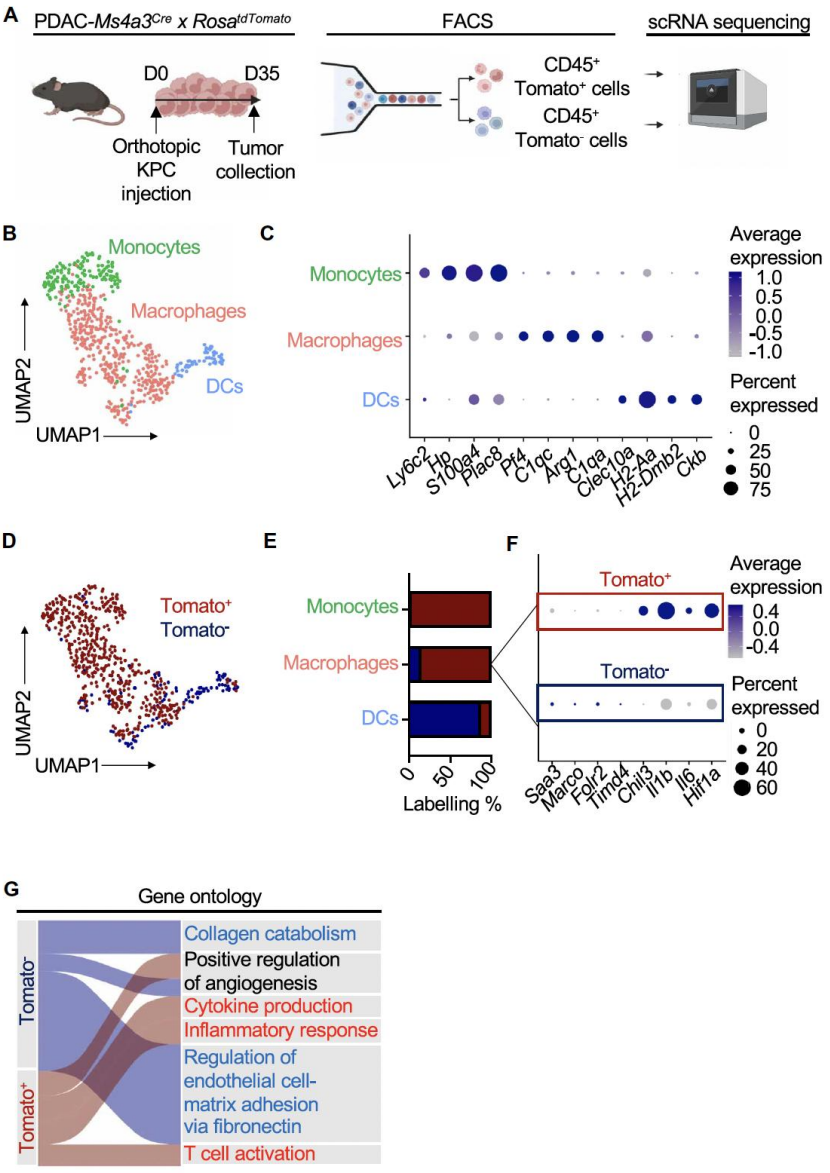


**Fig. 1. Ontogeny of TAMs influences their transcriptional profile.** (**A**) Experimental design of scRNA-seq of tumor tdTomato$^+$ and tdTomato$^-$ cells from *Ms4a3*$^{Cre}$ x *Rosa*$^{tdTomato}$ mice with KPC-derived PDAC ($n = 3$ mice, samples pooled). Tumors were collected at day 35 after tumor injection. FACS, fluorescence-activated cell sorting. (**B**) UMAP representation of the scRNA-seq data filtered on monocytes, macrophages, and DCs. (**C**) Dot plot showing top DEGs [false discovery rate (FDR) < 0.05 and highest logFC] from monocytes, macrophages, and DCs. (**D**) tdTomato protein labeling across sorted monocytes, macrophages, and DCs. (**E**) Proportions of monocytes, macrophages, and DCs labeled with tdTomato. (**F**) Dot plot showing leading DEGs from tdTomato$^+$ and tdTomato$^-$ macrophages. (**G**) Alluvial plot where bar thickness represents the enrichment of GO from tdTomato$^+$ and tdTomato$^-$ macrophages.

*Published in : Science Immunology (2024), vol. 9, eadk3981*
*DOI: 10.1126/sciimmunol.adk3981*
*Status : Postprint (Author's version)*

**TAMs are distinct from embryonically derived TAMs**

Because most TAMs in our PDAC model were of monocytic origin, we next investigated the dynamics of the monocyte- to- macrophage transition in these tumors using *Ms4a3*$^{CreERT2}$ x *Rosa*$^{tdTomato}$ mice. In this model, treatment with tamoxifen induces tdTomato expression in GMP- derived short- lived circulating Ly6C$^{hi}$ monocytes for 6 days, after which they are replaced in the circulation by newly generated tdTomato$^{-}$ cells (*13*). We injected KPC cells as described above and then administered tamoxifen on days 17/18 to induce GMP labeling midway through tumor growth to measure monocyte recruitment in an established tumor. At 35 days after injection of tumor cells, we harvested tumors and control healthy pancreases to characterize the immune cells present (both tdTomato$^{+}$ and tdTomato$^{-}$ cells) by scRNA- seq (Fig. 2A). We focused on mononuclear phagocyte subpopulations (fig. S2, A to C). After cell cluster annotation based on canonical differentially expressed genes (DEGs) (fig. S2D and data file S4), we identified five clusters that were enriched in PDAC: monocytes, TAM clusters 1 to 3, and dividing cells (fig. S2, E and F). Monocytes and TAMs clustered closely, indicating transcriptional similarities (fig. S2G), but with TAMs uniquely expressing specific markers, including *Arg1*, *Spp1*, and *Mmp12* (fig. S2H) (*16*–*18*).

Focusing on the PDAC- enriched monocyte and TAM populations, we visualized these subsets separately with uniform manifold approximation and projection (UMAP) and identified DEGs (Fig. 2, B and C, and data file S5). These populations were highly similar to previously described subsets, with TAM1s representing a population of monocyte- like TAMs that express *Tnf* and *Ccr2*, TAM2s being similar to hypoxic macrophages, and TAM3s resembling the previously described lipid- associated macrophages (LAMs) (*19*, *20*). To define developmental relationships between these clusters, we applied the splicing analytical tool scVelo (*21*) and found that monocytes putatively gave rise to TAM1s, which then differentiated into either TAM2s or TAM3s (Fig. 2D). These findings were recapitulated using the cell lineage and pseudotime inference tool Slingshot (Fig. 2E) (*22*). Therefore, TAM1s represent cells with a discrete but transient transcriptional state, likely constituting an intermediate stage between monocytes and TAM2/TAM3 differentiation (Fig. 2F).

To validate this hypothesis, we exploited the time-stamping feature of the model by comparing the proportion of tdTomato$^{+}$ cells in each TAM cluster. We observed fewer labeled TAM1s than TAM2s or TAM3s, confirming that the latter mainly derived from monocytes recruited shortly after the activation of tdTomato labeling on days 17/18, whereas by day 35, the TAM1 population was derived mostly from more recently recruited tdTomato$^{-}$ monocytes (Fig. 2, G and H). As expected, monocytes were mostly tdTomato$^{-}$ at the time of tumor collection, confirming their short life span and their continuous replenishment by GMPs. Therefore, by coupling scRNA-seq and monocyte time- stamping, we revealed a transient cell state in the monocyte- to- TAM transition and its subsequent differentiation into two distinct TAM populations.

*Published in : Science Immunology (2024), vol. 9, eadk3981*
*DOI: 10.1126/sciimmunol.adk3981*
*Status : Postprint (Author's version)*

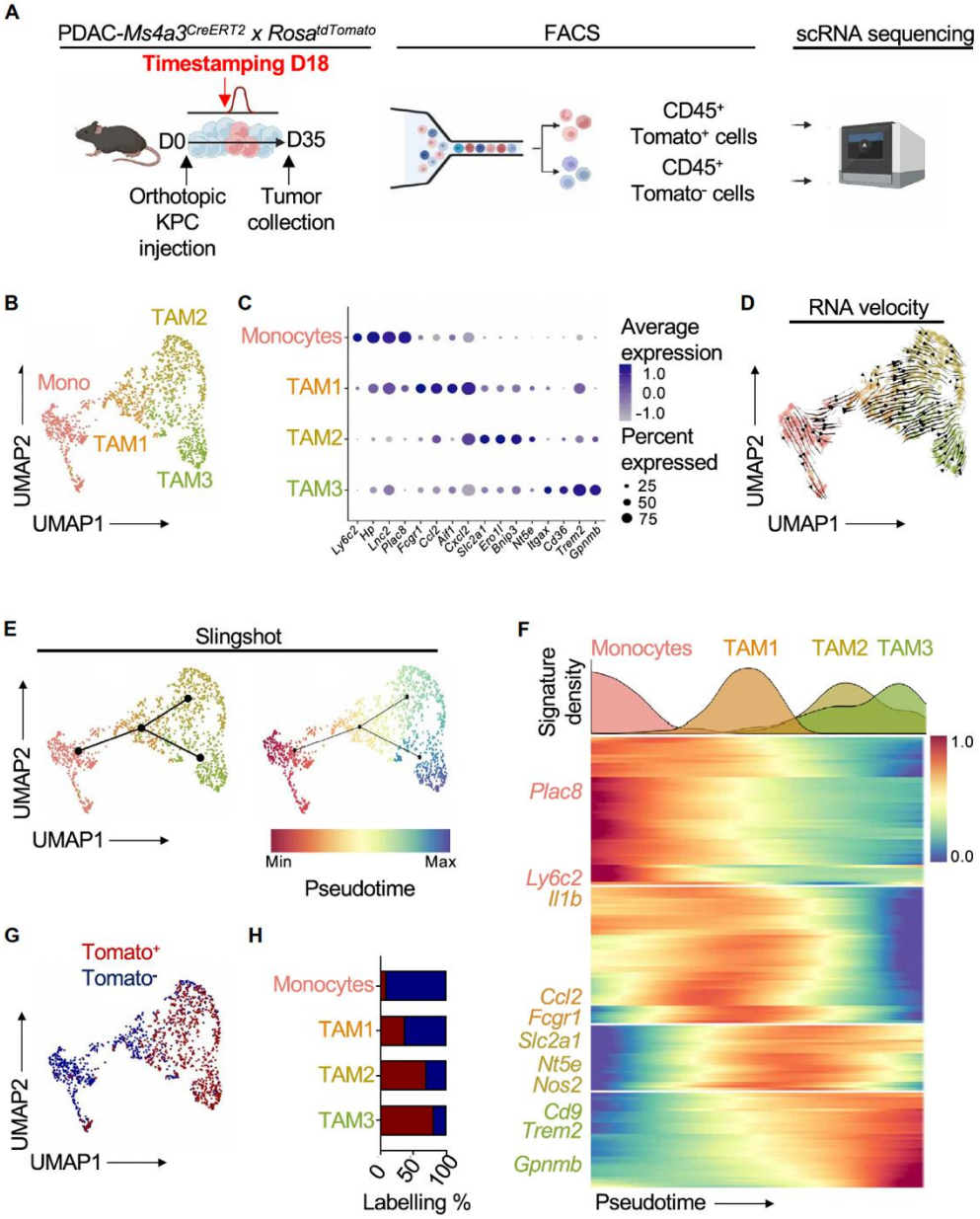


**Fig. 2. Time-stamping reveals temporal relationships of TAM populations.** (**A**) Experimental design of scRNA-seq of tumor tdTomato$^+$ and tdTomato$^-$ cells from *Ms4a3*$^{CreERT2}$ x *Rosa*$^{tdTomato}$ mice with KPC-derived PDAC, pulsed with tamoxifen at day 18 after tumor injection ($n = 3$ mice, samples pooled). (**B**) UMAP representation of the scRNA-seq data filtered on monocytes, TAM1s, TAM2s, and TAM3s. (**C**) Dot plots of top DEGs from monocytes, TAM1s, TAM2s, and TAM3s. (**D**) UMAP with arrows showing the scVelo analysis of monocyte-to-macrophage differentiation. (**E**) UMAP showing clustering and pseudotime analysis of monocytes, TAM1s, TAM2s, and TAM3s. (**F**) Heatmap of ordered pseudotime analysis from Slingshot and signature density of monocytes, TAM1s, TAM2s, and TAM3s. (**G**) UMAP showing *Ms4a3*$^{CreERT2}$ x *Rosa*$^{tdTomato}$ labeling of monocytes, TAM1s, TAM2s, and TAM3s. tdTomato labeling is based on the FACS sorting. (**H**) Proportions of *Ms4a3*$^{CreERT2}$ x *Rosa*$^{tdTomato}$ labeling of monocytes, TAM1s, TAM2s, and TAM3s.

*Published in : Science Immunology (2024), vol. 9, eadk3981*
*DOI: 10.1126/sciimmunol.adk3981*
*Status : Postprint (Author's version)*

**High-throughput screening identifies surface markers associated with monocyte and TAM subpopulations**

To enable further study and validation of these TAM clusters, we used the Infinity Flow pipeline (*23*, *24*) to assess the expression of surface markers on monocytes and TAM1s to TAM3s. We first injected KPC cells into the pancreases of $Ms4a3^{CreERT2}$ x $Rosa^{tdTomato}$ mice; treated them with tamoxifen during early (days 14/15), intermediate (days 21/22), or late (days 28/29) stages of tumor establishment; and then collected, barcoded, and labeled tumor cells at day 35 to assess surface expression of 270 proteins detectable by flow cytometry (Fig. 3A).

tdTomato labeling of monocytes and TAMs exhibited the expected pattern: Labeled monocytes (Ly6C$^+$) were evident after late tamoxifen treatment, confirming their short life span, whereas TAM (CD64$^+$ F4/80$^+$) labeling was less pronounced, mirroring the continuous monocyte- to- macrophage transition in tumors (fig. S3A). Considering only tdTomato$^+$ monocytes and TAMs, we generated a UMAP on the basis of the flow cytometry data and identified four clusters that we annotated as monocytes and TAM1s to TAM3s on the basis of similarities between their patterns of gene (Fig. 2) and protein expression (Fig. 3B and fig. S3, B and C). Thus, we defined monocytes as Ly6C$^+$, TAM1s as CCR2$^+$ CD64$^+$, TAM2s as CD73$^+$, and TAM3s as CD36$^+$ CD11c$^+$ cells (Fig. 3C and data file S6). Using these markers, we established a gating strategy to discriminate monocytes, TAM1s, TAM2s, and TAM3s using a limited panel of surface markers that enable detection of the populations of interest by conventional spectral flow cytometry (Fig. 3D and fig. S3, D and E). To verify the accuracy of this gating strategy and validate our scRNA-seq, we sorted Ly6C $^+$ monocytes, TAM1s, TAM2s, and TAM3s and profiled them by bulk RNA sequencing. Each sorted population had a distinct transcriptional profile that corresponded to its respective cluster of interest when their signatures were projected back onto the scRNA- seq data (fig. S4, A and B). We then compared the relative abundance of each of these populations within all tdTomato$^+$ mononuclear phagocytes at different time points, revealing an enrichment in monocytes and TAM1s at the late time point of monocyte time-stamping. In contrast, the early time point was almost exclusively composed of TAM2s and TAM3s (Fig. 3, E and F). The trajectory of monocytes to a transient TAM1 state and subsequentially TAM2s and TAM3s was also confirmed by applying Slingshot analysis to these surface marker data (Fig. 3, G and H). These results validated those generated from gene expression and confirmed at the protein level the temporal relationship between monocytes and the different TAM subpopulations. Because the TAM1 population constitutes an intermediate precursor of more stable TAM2 and TAM3 macrophage populations, we propose the nomenclature intermediate TAM (IntTAM) for these cells.

*Published in : Science Immunology (2024), vol. 9, eadk3981*
*DOI: 10.1126/sciimmunol.adk3981*
*Status : Postprint (Author's version)*

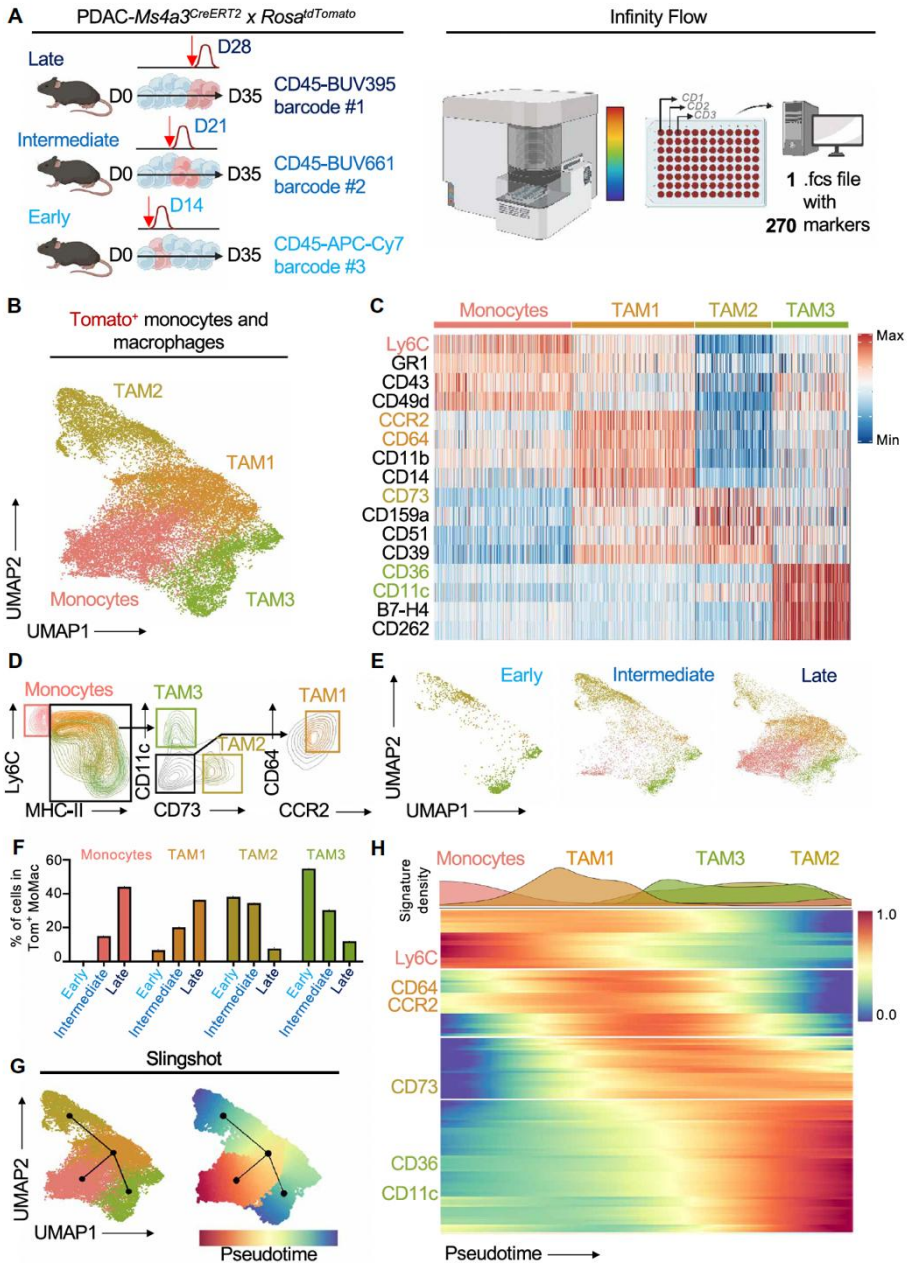


**Fig. 3. Surface marker identification and dynamic time-stamping of TAM subpopulations.** (**A**) Experimental design of LEGENDscreen analysis from *Ms4a3*$^{CreERT2}$ x *Rosa*$^{tdTomato}$ mice pulsed with tamoxifen at days 14, 21, and 28 after orthotopic injection of KPC cells ($n$ = 3 mice for each time point). (**B**) UMAP of tdTomato-labeled monocytes and macrophages from the Infinity Flow analysis labeled as monocytes, TAM1s, TAM2s, and TAM3s. (**C**) Top differentially expressed proteins (top five logFC and FDR > 0.05) in monocytes, TAM1s, TAM2s, and TAM3s. (**D**) Gating strategy identifying monocytes, TAM1s, TAM2s, and TAM3s. (**E**) UMAP showing the different clusters present at late (day 28), intermediate (day 21), and early (day 14) tdTomato$^{+}$ mononuclear cells. (**F**) Proportion of clustered cells in late (day 28), intermediate (day 21), and early (day 14) time points. (**G**) UMAP of Slingshot analysis with lines showing start and end points and pseudotime analysis. (**H**) Heatmap of ordered pseudotime analysis from Slingshot and signature density of monocytes, TAM1s, TAM2s, and TAM3s.

*Published in : Science Immunology (2024), vol. 9, eadk3981*
*DOI: 10.1126/sciimmunol.adk3981*
*Status : Postprint (Author's version)*

**IntTAMs give rise to TAM2s and TAM3s, which are differentially regulated by Maf**

We next asked how the relative proportions of monocytes and TAM subpopulations varied during PDAC development. As expected, monocytes, IntTAMs, TAM2s, and TAM3s were more abundant in tumors compared with those in adjacent/healthy pancreas (fig. S5A). However, these populations exhibited dynamic changes during tumor development: IntTAM abundance peaked at 7 days after tumor initiation, whereas TAM2s and TAM3s became more abundant as the tumor developed (fig. S5, B to D), consistent with our hypothesis of their sequential differentiation from IntTAMs.

To further validate the dependence of TAM populations on monocyte differentiation, we orthotopically injected KPC cells into *Ccr2*–knockout (KO) mice. After 3 weeks after challenge, we observed that monocytes, IntTAMs, TAM2s, and TAM3s, but not RTMs, were all reduced in *Ccr2*- KO mice compared with those in wild-type (WT) mice (fig. S6A). To precisely define the transition of monocytes to TAMs, we treated PDAC- bearing $Ms4a3^{CreERT2}$ x $Rosa^{tdTomato}$ mice with tamoxifen at various time points to provide sequential monocyte time-stamping and then applied the conventional flow cytometry gating strategy to tumor samples (Fig. 4A). IntTAMs were mostly labeled after late tamoxifen induction, indicative of recent recruitment (Fig. 4B). Conversely, TAM2s and, to a lesser extent, TAM3s were mostly labeled after early induction, suggesting their long survival and their differentiation from early recruited monocytes (Fig. 4B). As mentioned above, previous studies reported a population of *Trem2*- expressing macrophages called LAMs in several diseases, including cancer (*20*, *25*–*27*). On the basis of our gene and protein expression data, we hypothesized that TAM3s were equivalent to these TREM2$^+$ LAMs. We tested this hypothesis by initiating PDAC in $Trem2^{EGFP}$ reporter mice and found that TAM3s were specifically labeled (fig. S6, B and C).

To validate the potential of IntTAMs to differentiate into TAM2s and TAM3s, we sorted IntTAMs from tumor-bearing CD45.2 mice (21 days after orthotopic tumor injection) and adoptively transferred them intratumorally into tumor- bearing CD45.1 mice (21 days after orthotopic tumor injection). We analyzed the progeny of adoptively transferred CD45.2$^+$ cells at day 3 and day 7 after the transfer by flow cytometry (Fig. 4C). The majority of CD45.2$^+$ cells remained IntTAMs at day 3 but had then converted into TAM2s and TAM3s by day 7 after transfer (Fig. 4D and fig. S7A), validating the potential of IntTAMs to give rise to both TAM2s and TAM3s.

To better understand the transcriptomic identities and putative functions of monocytes, IntTAMs, TAM2s, and TAM3s in PDAC, we applied the SCENIC analytical tool to our scRNA- seq data to predict transcription factor activity based on gene expression (*28*). This analysis revealed distinct regulons in the different cell populations: Whereas monocytes preferentially used *Irf1*- and *Klf3*- related genes, IntTAMs rather used those related to *Fosl2*; TAM2s used *Maf*- and *Irf8*- related genes, and TAM3s used genes related to *Bhlhe41* (Fig. 4E). After our identification of *Maf* as a potential regulator of TAM2 differentiation, we used a $LysM^{cre}$ x $Maf^{flox}$ mouse model to investigate whether TAM differentiation was altered. Mice with *Maf*- deficient myeloid cells exhibited a substantial reduction in TAM2 but not in tumor growth (Fig. 4, F and G). These results suggest that targeting transcription factors can modulate the differentiation of TAM subpopulations.

*Published in : Science Immunology (2024), vol. 9, eadk3981*
*DOI: 10.1126/sciimmunol.adk3981*
*Status : Postprint (Author's version)*

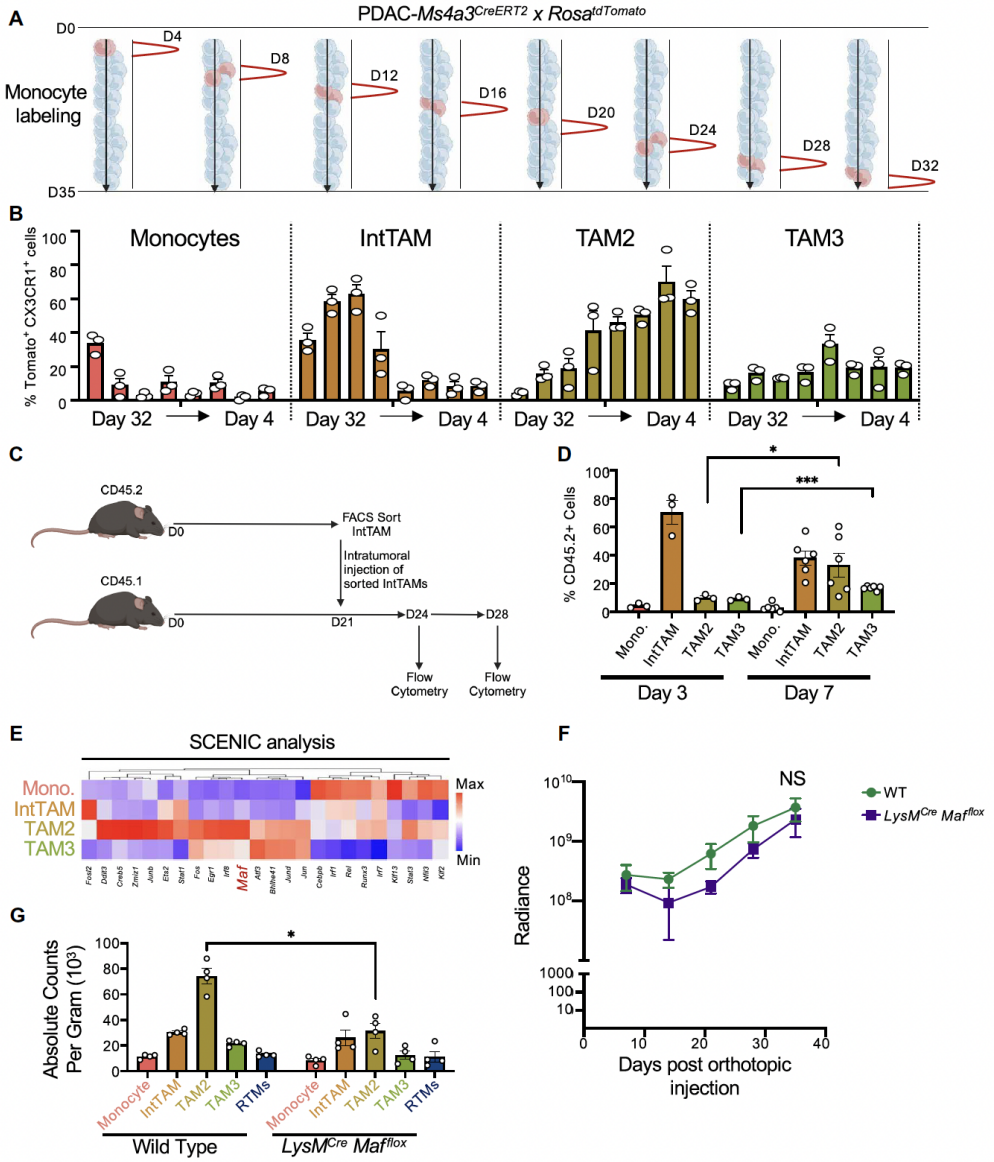


**Fig. 4. IntTAMs give rise to *Maf*-dependent TAM2s and *Maf*-independent TAM3s.** (**A**) Experimental design of time-stamping *Ms4a3*$^{CreERT2}$ *Rosa*$^{tdTomato}$ mice every 4 days after tumor injection. All mice were sacrificed at day 35, and tissues were digested for spectral flow cytometry. (**B**) Proportion of tdTomato labeling of monocytes, IntTAMs, TAM2s, and TAM3s at each time point of tamoxifen administration. (**C**) Experimental design of intratumoral adoptive transfer of IntTAMs into mice with KPC-derived PDAC. (**D**) Immunophenotyping of adoptively transferred IntTAMs at day 3 or 7 after transfer. (**E**) SCENIC analysis predicting differentially expressed regulons in different monocyte and TAM populations. (**F**) Tumor growth curve of *LysM*$^{Cre}$ x *Maf*$^{flox}$ and WT mice ($n$ = 3 or 4 mice per group). (**G**) Cumulative results of the abundance of each TAM population in *LysM*$^{Cre}$ x *Maf*$^{flox}$ and WT mice. Statistics were performed using a Mann-Whitney test. *$P < 0.05$ and ***$P < 0.001$.

*Published in : Science Immunology (2024), vol. 9, eadk3981*
*DOI: 10.1126/sciimmunol.adk3981*
*Status : Postprint (Author's version)*

**IntTAMs, TAM2s, and TAM3s have distinct motility and cellular interaction profiles**

To further understand the functional potential of TAM subsets, we performed GO analysis using MetaScape (*29*). Genes expressed by IntTAMs were associated with chemotaxis, those by TAM2s with hypoxia, and TAM3s expressed genes involved in the response to lipoproteins (fig. S8A). Given the evolving gene scores for these pathways during the monocyte- to- TAM differentiation, it seems that IntTAMs start to express the chemotaxis- associated program when differentiating from monocytes, presumably allowing them to migrate within the tumor to a site in which this initial program is gradually replaced by either the hypoxia-associated identity of TAM2s or the response- to- lipoprotein–associated identity of TAM3s (fig. S8B).

To further investigate the predicted role of IntTAMs, we sorted monocytes, IntTAMs, TAM2s, and TAM3s and measured their motility capacity. Monocytes had the highest motility capacity, whereas IntTAM had an intermediate motile capacity, and TAM2s and TAM3s had a comparatively reduced ability to move (fig. S8, C and D). These results suggest that IntTAMs display an intermediate motility in the monocyte- to- macrophage transition, still endowed with migration ability compared with long-lived differentiated TAM2s and TAM3s. Once IntTAMs have moved through tissue and further matured, thus losing their motile capacity, we questioned whether the role of spatial localization could influence the functional profiles of TAM subpopulations. To do so, we used our scRNA- seq data and integrated them with a publicly available scRNA- seq dataset to predict interactions between the different subpopulations with other components of the TME (fig. S9, A and B) (*30*, *31*). To identify outgoing and incoming interactions in monocytes, IntTAMs, TAM2s, and TAM3s, we calculated the number of significant interactions between cell types and found distinct preferential interactions (fig. S9C). Together, these results suggest that the distinct TAM populations could interact with different cell types in a specific tumoral niche, subjecting them to distinct influences and microenvironmental factors that could contribute to their differentiation and functional profiles.

**TAM2s and TAM3s are associated with distinct spatial niches in PDAC**

Because our gene score analysis suggested the possibility of differential localization and functional specialization of TAM populations in PDAC, we next asked whether there was in vivo evidence for this by analyzing recently published spatial transcriptomics data (Visium, 10x Genomics) collected on sections of PDAC tumors (Fig. 5A) (*32*). Using BayesSpace joint clustering (*33*), we identified seven distinct spatial clusters corresponding to seven tumor niches associated with different gene expression and putative functions (Fig. 5, B and C; fig. S10, A and B; and data file S7): Cluster 1 was associated with hypoxia, cluster 3 with cellular respiration, cluster 4 with RNA splicing, cluster 5 with inflammatory response, cluster 6 with telomere lengthening, and cluster 7 with cell cycle, whereas cluster 2 was excluded from the analysis because of its restriction to necrotic areas and lower- quality sequencing data (Fig. 5C). Using BayesSpace, we also projected genes associated with each cell type to predict the presence of multiple immune and nonimmune cell types in the tumor (fig. S10C). We also projected the signatures of IntTAMs, TAM2s, and TAM3s (Fig. 5D) and measured their proportions in each cluster from the different tissue sections. TAM2s were significantly enriched across all tissue sections in the

*Published in : Science Immunology (2024), vol. 9, eadk3981*
*DOI: 10.1126/sciimmunol.adk3981*
*Status : Postprint (Author's version)*

cluster 1 hypoxic tissue, suggesting an association between low oxygen levels and the TAM2 program (Fig. 5, E and F). A mutual exclusion of TAM2s and TAM3s was observed (fig. S10D). Therefore, these results suggest that differentiated TAM2 and TAM3 populations inhabit distinct niches within the tumor.

To validate the distribution of these populations at the protein level, we used codetection by indexing (CODEX)–enabled high- dimensional histology (*34*). First, we annotated tumor regions using hematoxylin and eosin (H&E) staining. Next, using a 58- parameter staining panel, we identified cell types using common markers and the gating strategy previously identified by flow cytometry (Fig. 5G and fig. S11, A and B). Here, CODEX analysis revealed that TAM2s were in closer proximity to the necrotic core of the tumor, whereas TAM3s were distributed further from the tumor core (Fig. 5H and fig. S11C), in agreement with our spatial transcriptomic analysis. To identify the cell interactions between TAMs and the TME, we identified regions where each TAM population was present (fig. S11D). Region 1 was enriched with IntTAMs, region 2 with monocytes, region 3 with TAM2s, and region 4 with TAM3s (fig. S11E). Within regions 3 and 4, fibroblasts, neutrophils, and B cells interacted frequently with TAM2s, whereas TAM3s interacted with cancer cells, natural killer (NK)/T cells, and DCs (fig. S11, F and G). The interaction of TAM2s with neutrophils parallels recent findings that the hypoxic regions of the tumor can also reprogram neutrophils that affect their functions (*32*). Together, these observations integrate time and space dimensions to reveal the fate of monocytes recruited in PDAC, highlighting a transient population of IntTAMs that give rise to two distinct stable TAM populations occupying different locations within the TME and exhibiting patterns of gene expression consistent with distinct functional specializations.

*Published in : Science Immunology (2024), vol. 9, eadk3981*
*DOI: 10.1126/sciimmunol.adk3981*
*Status : Postprint (Author's version)*

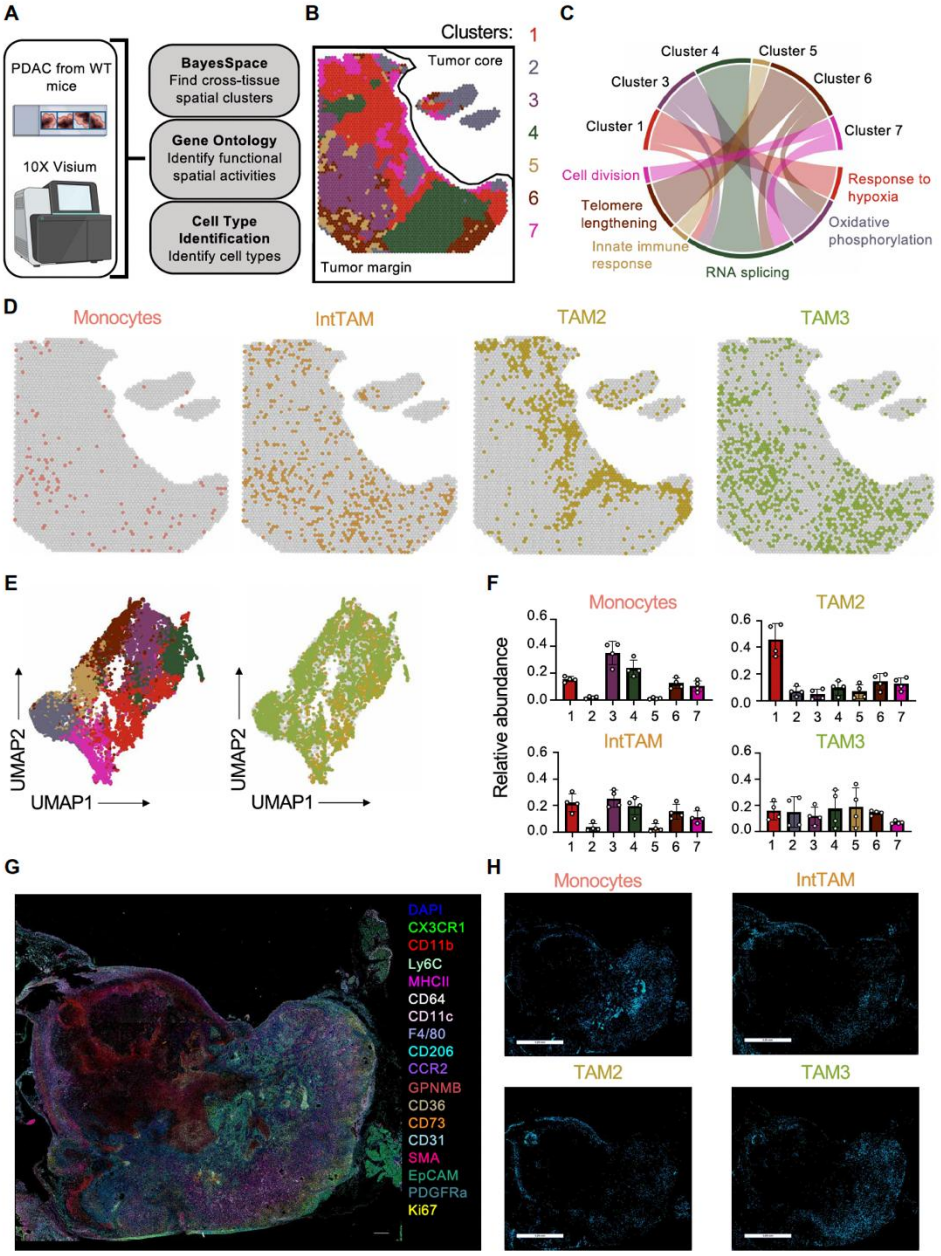


**Fig. 5. TAM2s and TAM3s inhabit distinct niches in PDAC.** (**A**) Experimental outline of 10x Visium spatial transcriptomics sample preparation and data analysis of KPC-derived PDAC in WT mice at either day 14 or day 42 ($n = 4$ mice). (**B**) Clustering and functional annotation of tumor areas. (**C**) Circo plot with bar thickness representing the enrichment score of GO for each spatial cluster. (**D**) Projection of monocyte, IntTAM, TAM2, and TAM3 signatures on the tumor sample (**E**) UMAP of spatial clusters and predicted cell types from 10x Visium analysis. (**F**) Abundance of monocytes, IntTAMs, TAM2s, and TAM3s in each spatial cluster. (**G**) CODEX analysis with stromal and immune markers used to identify populations of cells in murine PDAC. (**H**) Density plots from multiplex CODEX imaging analysis representing IntTAMs, TAM2s, and TAM3s. Scale bars, 3.25 mm.

*Published in : Science Immunology (2024), vol. 9, eadk3981*
*DOI: 10.1126/sciimmunol.adk3981*
*Status : Postprint (Author's version)*

**Human PDAC contains TAM subpopulations that transcriptionally and spatially correspond to murine TAMs**

Last, we assessed whether similar macrophage populations were present in patients with PDAC. Using publicly available scRNA-seq data from human PDAC and adjacent healthy pancreas (*35*–*38*), we identified mononuclear phagocytes and applied clustering analysis (Fig. 6A). This revealed one population of monocytes and eight populations of human TAMs (Hu.TAMs a to h) (Fig. 6B) with distinct transcriptomic identities (fig. S12A and data file S8) that were identifiable in every dataset representing 96 patients (fig. S12B). In tumor tissue, there was an enrichment of Hu.TAMs a to f compared with the adjacent healthy tissue (Fig. 6C). We then performed a label transfer pairing analysis (*39*) that revealed marked transcriptional similarities between murine and human monocytes, murine IntTAMs and Hu.TAM a, murine TAM2s and Hu.TAMs b/c, and murine TAM3s and Hu.TAMs d/e (Fig. 6D). We did not find an ortholog of the Hu.TAM f population, suggesting species specificity that warrants further exploration on TAM populations. When we projected DEGs across monocytes and TAMs in mouse and human PDAC, we observed a similar gene expression on clustering between the species (Fig. 6E), as well as conserved functional pathways between paired populations (fig. S12C).

To address whether monocyte- derived TAMs had a similar differentiation trajectory in human PDAC, we used PAGA to predict the differentiation pathway of monocytes to TAMs (*40*). We found that monocytes connected first to Hu.TAM a and then further differentiated into different TAMs (Fig. 6F). Furthermore, using pseudotime analysis, we observed the putative differentiation of monocytes to Hu.TAM a and then to Hu.TAMs b/c or Hu.TAMs d/e along with genes identified to be associated with each population (Fig. 6G). To further confirm these observations, we projected the DEGs of human monocytes treated with M- CSF for 0, 3, 9, 24, and 48 hours (*41*). We found that, initially, monocytes displayed their classic signature, and, after 3 hours, the signature overlapped with Hu.TAM a. Subsequent time points showed overlap with different Hu.TAM populations, further supporting that Hu.TAM a emerges first and gives rise to other Hu.TAM populations (fig. S12D).

Using a publicly available PDAC NanoString Digital Spatial Profiler (DSP) dataset (GSE199102) (*35*), which allows the transcriptomic characterization of tumor ($PanCK^+$) and immune ($CD45^+$) cells within regions of interest (ROIs) on tissue slices, we then predicted the presence of macrophage signatures in different parts of PDAC tissue. We deconvoluted the $CD45^+$ fraction of each ROI to evaluate the presence of monocytes, Hu.TAM a, Hu.TAMs b/c, and Hu.TAMs d/e using the DEGs of each population. In parallel, we tracked hypoxic or lipid metabolism signatures in the $PanCK^+$ fractions using publicly available gene sets from gene set enrichment analysis (GSEA) (*42*, *43*). We then correlated these two layers to identify any association between TAM populations and environmental tumor phenotypes. As observed in murine PDAC, we found that tumor areas with a high score for hypoxia also had a high signature of Hu.TAMs b/c, whereas the localization of other TAM populations was not significantly related to different functional signatures (fig. S13A).

*Published in : Science Immunology (2024), vol. 9, eadk3981*
*DOI: 10.1126/sciimmunol.adk3981*
*Status : Postprint (Author's version)*

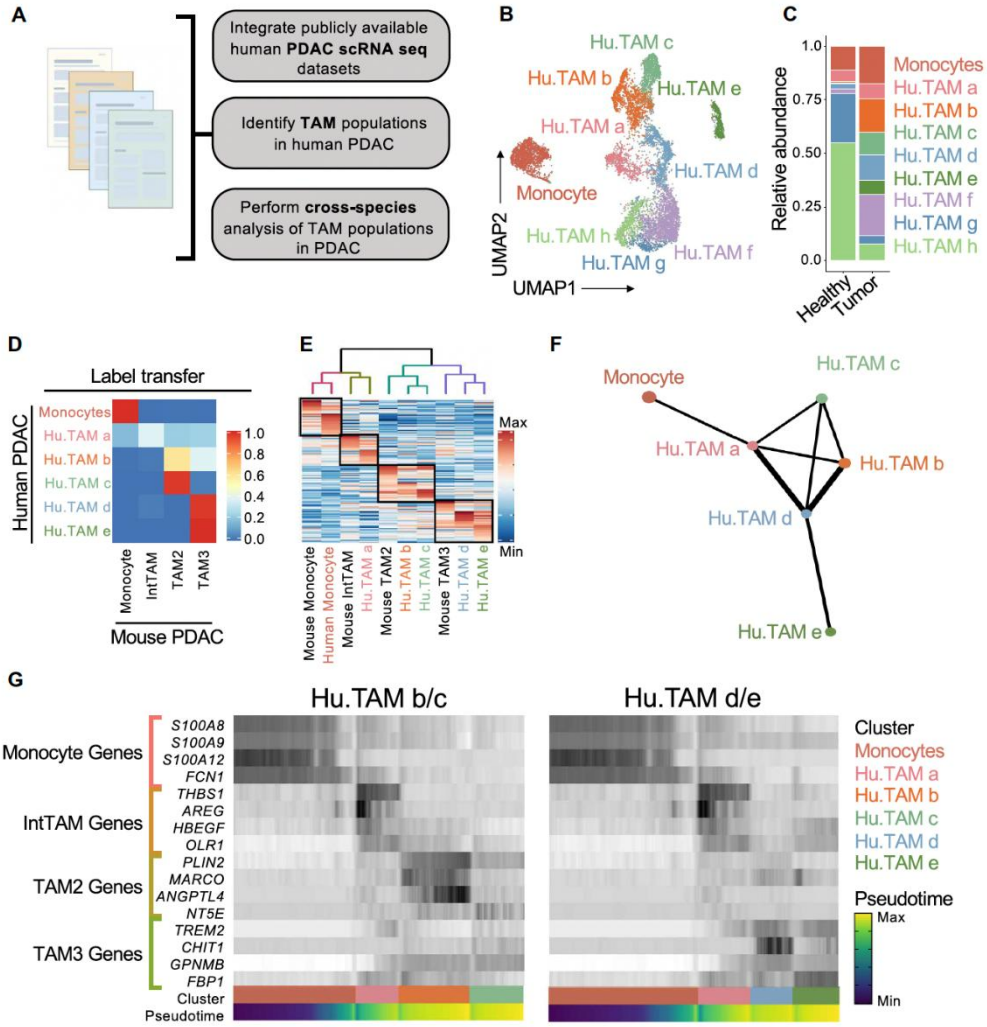


**Fig. 6. Identification of TAM subpopulations in human PDAC.** (**A**) Integration and analysis of human PDAC analysis from previously published datasets containing a total of seven healthy patient samples and 89 PDAC samples (*35*–*38*). (**B**) Identification of clusters corresponding to monocyte and Hu.TAM populations a to h. (**C**) Proportions of monocytes and Hu.TAMs a to h across control and tumor tissues. (**D**) Label transfer of monocyte and TAM populations in murine PDAC to populations identified in human PDAC. (**E**) Clustering and shared gene expression of monocytes and TAM populations in mouse and human PDAC. (**F**) PAGA analysis showing the link between the monocytes and TAM populations. (**G**) Heatmaps showing the differentiation of monocytes to TAMs.

On the basis of this transcriptional homology, we used our murine surface marker analysis to define putative markers for the Hu.TAM subpopulations (fig. S13B and data file S9). We annotated viable and necrotic regions of human PDAC tissues and identified Hu.TAM a ($CCR2^+$ $CD68^+$), Hu.TAMs b/c ($CD68^+$ $CD73^+$), and Hu.TAMs d/e ($CD68^+$ $TREM2^+$) (Fig. 7, A and B). In tumor sections, these populations were localized within different areas, with Hu.TAMs b/c enriched in the necrotic tumor (Fig. 7C). Moreover, by investigating the proximity of one TAM population to another, we found that Hu.TAMs b/c and Hu.TAMs d/e localized further away from one another, suggesting a pattern of spatial segregation similar to those in murine PDAC (Fig. 7D).

Last, we asked whether the expression of TAM subpopulation- specific/related genes correlated with prognosis of patients with PDAC. We normalized monocyte and Hu.TAM abundance with a

*Published in : Science Immunology (2024), vol. 9, eadk3981*
*DOI: 10.1126/sciimmunol.adk3981*
*Status : Postprint (Author's version)*

Dirichlet- multinomial regression comparing patient response to standard PDAC treatment (FOLFIRINOX, 5-FU, radiotherapy, and Losartan in few patients) (*35*). We found that most Hu.TAM populations were reduced upon treatment; however, in poor responders, we observed a persistence in the abundance of Hu.TAMs c, d, and e (fig. S13C). In addition, we screened the 30 most DEGs from each TAM population using the Cancer Genome Atlas (TCGA) database (*44*) and found that high expression of the Hu.TAM b/c signature was significantly associated with shorter survival of patients with PDAC (Fig. 7E and fig. S13D). Together, these results suggest that the abundance of different TAM populations could be used as a tool for patient prognosis.

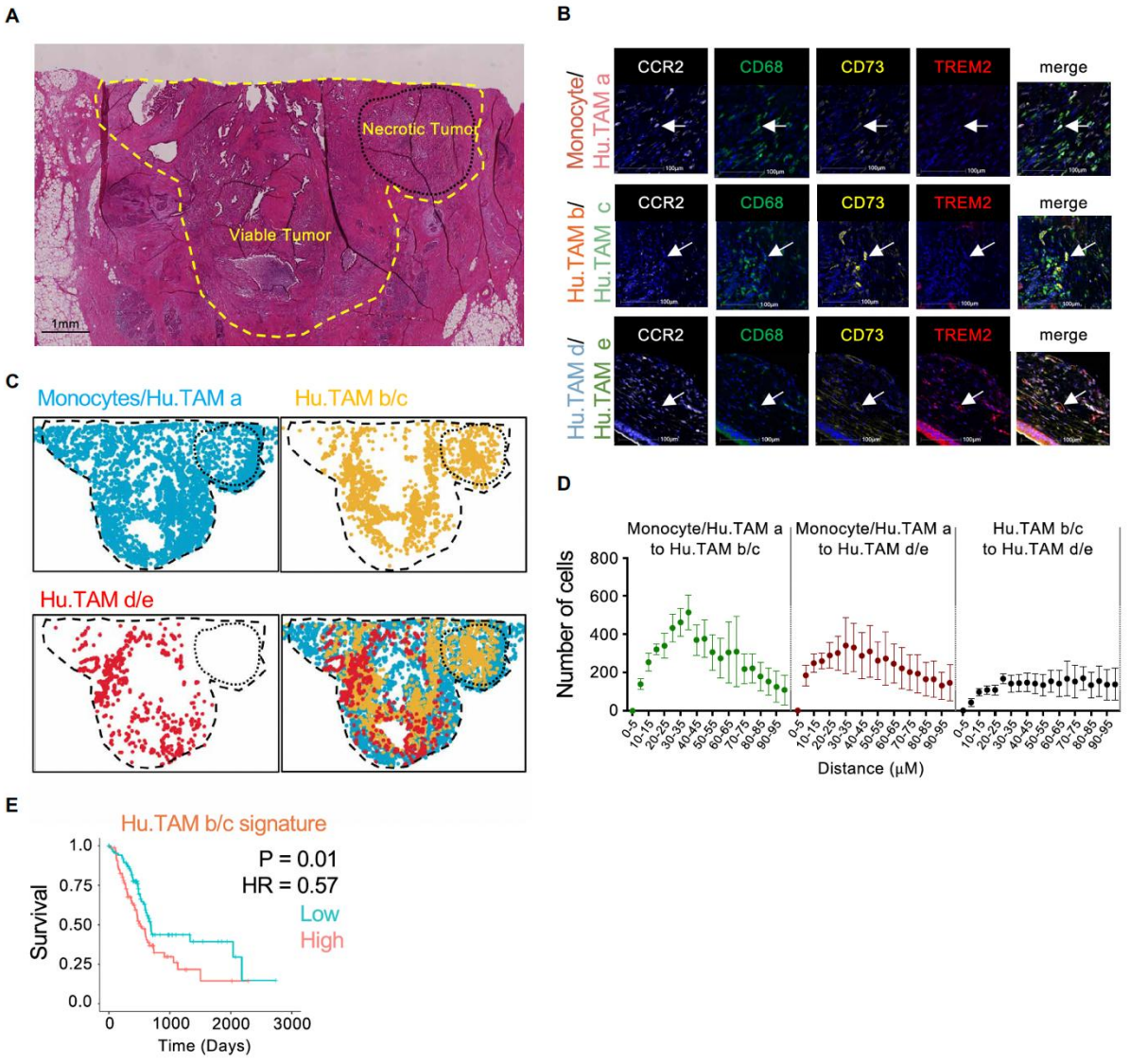


**Fig. 7. TAMs have distinct spatial distribution in human PDAC.** (**A**) H&E staining of human PDAC tissue with annotation of viable and necrotic tumor tissue. (**B**) Immunofluorescence of markers identifying monocytes and macrophages in human PDAC. Arrows point to monocyte/Hu.TAM a, Hu.TAMs b/c, and Hu.TAMs d/e. (**C**) Dots representing different macrophage populations identified in human PDAC tissue. (**D**) Proximity of monocyte and TAM populations to one another ($n = 4$ different human PDAC tissues). (**E**) Survival curve of data from the TCGA representing the impact of the Hu.TAM b/c signature on patient survival. HR, hazard ratio.

*Published in : Science Immunology (2024), vol. 9, eadk3981*
*DOI: 10.1126/sciimmunol.adk3981*
*Status : Postprint (Author's version)*

# DISCUSSION

Herein, we combined fate-mapping and time- stamping *Ms4a3*- derived mouse models and multiomics analyses to track monocytes entering PDAC to precisely analyze the dynamics of their differentiation into TAMs. In this context, we identified a discrete intermediate population in the transition from monocytes to macrophages, both in murine and human pancreatic tumors. Although the impact of ontogeny on TAM functions has been well studied during the last decade, little is known about the differentiation paths of TAM populations. Herein, we have addressed this gap of knowledge using our time- stamping model, which represents the overcoming of a significant technological barrier. A recent study observed a cell population that resembles IntTAMs by the expression of CCR2 and CD64 within inflamed blood vessels but did not acknowledge the transitional capacity of these cells (*45*). In addition, although IntTAMs exhibit a proinflammatory phenotype, their exact contribution to tumor- derived inflammation should be investigated in future works.

Our results suggest that transient IntTAMs give rise to more mature TAM2s or TAM3s, with their phenotype predominantly governed by their local environment. Given these observations, we propose that a major determinant of macrophage phenotype in cancer is the availability of nutrients. The TAM3 population that we observed in PDAC has been implicated in immunomodulatory functions, as reported by others, albeit without temporal assessment (*26*, *46*). TAM3s express the lipid-binding gene *Trem2*: Macrophages expressing this gene engage in lipid metabolism (*20*). Recent work suggests that the phagocytosis of tumor cells drives the emergence of $Trem2^{+}$ macrophages in a murine model of lung adenocarcinoma and prevents NK cell recruitment (*25*). In addition, the tumors of *Trem2*-deficient mice, which have few $TREM2^{+}$ macrophages, are more responsive to anti–PD- 1 treatment (*26*).

Conversely, IntTAMs can also give rise to TAM2s, which may be driven by hypoxia. Accordingly, the transcription factor Hif1α, a primary regulator of hypoxia-induced programs, is expressed by TAM2s. Previous work showed that hypoxia-associated macrophages con- tribute to immune suppression (*47*), and, here, we see that increased abundance of these hypoxia- associated TAM2s is linked with poor patient prognosis. Our observations are recapitulated in a recent study where spatially restricted TAM populations in a variety of cancers are associated with hypoxia and poor prognosis (*48*). Together, this feature argues for specific TAM2 targeting, potentially using hypoxia program inhibitors (*49*). Furthermore, we can inhibit the differentiation of IntTAMs to TAM2s by modulation *Maf* expression in $LysM^{cre}$ x $Maf^{flox}$ mice. Although these results do not show a significant change in tumor growth, they provide a proof of concept that modulation of downstream transcription factors can affect populations that arise from IntTAM without affecting other populations.

Our work positions IntTAMs as a distinct cell type with the capacity to integrate environmental signals to facilitate the transition from a monocyte to a specialized macrophage. This feature of IntTAMs alludes to a possible stage of macrophage differentiation that could be manipulated by therapeutic targeting. Future work could target IntTAMs and skew their differentiation to benefit patient outcome. In conclusion, this work and others highlight the need for a more refined definition

*Published in : Science Immunology (2024), vol. 9, eadk3981*
*DOI: 10.1126/sciimmunol.adk3981*
*Status : Postprint (Author's version)*

of TAM populations to enable the identification of critical targets for more effective immunotherapies and integrate time as a key parameter when considering TAM biology (*50*).

# MATERIALS AND METHODS

### Study design

Macrophages are an abundant immune cell type in many tumors and are often associated with poor prognosis; however, the inherent heterogeneity of these cells makes them challenging to study. To address this, we propose that ontogeny, time, and location affect the heterogeneity of macrophages in PDAC. We used $Ms4a3^{Cre}$ $Rosa^{tdTomato}$ mice to identify the ontogeny of macrophages, $Ms4a3^{CreERT2}$ $Rosa^{tdTomato}$ mice to investigate the impact of time on monocyte- derived macrophages, and spatial transcriptomics/multiplex imaging to evaluate the influence of location on macrophage heterogeneity.

### Mouse models

$Ms4a3_{Cre}$ x $Rosa_{tdTomato}$ and $Ms4a3_{CreERT2}$ x $Rosa_{tdTomato}$ mice were described previously (*13*). For tamoxifen treatment, mice were twice administered 1.75 mg of tamoxifen in 100 µl of corn oil by oral gavage 24 hours at the indicated time points after tumor cell injection. This study used healthy male and female mice for experimentation at 7 to 10 weeks of age. *Ccr2*-KO mice were provided by the laboratory of M. Lecuit (*51*). $LysM^{Cre}$ x $Maf^{flox}$ mice were from the laboratory of T. Marichal (*52*). Mice housed and bred at Institut Gustave Roussy were kept and maintained according to the national recommendations. All protocols were approved by the Institutional Animal Care and Use Committee (IACUC) (approval number 202102240810563). All experiments and procedures performed at the Shanghai Jiao Tong University School of Medicine animal facility, Cyagen Inc., Shanghai, were approved by the IACUC of Shanghai Jiao Tong University School of Medicine. All experiments and procedures performed on mice housed at the Singapore Immunology network were approved by the IACUC of the Biological Resource Center (Agency for Science, Technology and Research, Singapore) following the guidelines of the Agri-Food and Veterinary Authority and the National Advisory Committee for Laboratory Animal Research of Singapore. All experiments presented here were performed on equal numbers of male and female mice.

### Orthotopic injection of KPC tumor cells

The murine PDAC cancer cell line $P48^{Cre}$ $Kras^{G12D/+}$ $Trp53^{R172H/+}$ (KPC) was a gift from the W. S. Cheng laboratory (Singapore Immunology Network, A*STAR, Singapore) (*53*). Before using KPC cells for experiments, they were passaged more than six times. Briefly, 50,000 cells were resuspended in 20 µl of ice- cold phosphate- buffered saline (PBS) and 25% Matrigel (Sigma- Aldrich) and were orthotopically injected into the pancreases of isoflurane- anaesthetized healthy 7- to 10- week animals as previously described (*54*). Immediately after surgery, buprenorphine (10 mg/kg) was subcutaneously

*Published in : Science Immunology (2024), vol. 9, eadk3981*
*DOI: 10.1126/sciimmunol.adk3981*
*Status : Postprint (Author's version)*

administered to mice, which were then monitored for the three subsequent days. All mice were sacrificed within 6 weeks of surgery. In addition, KPC cells used for these experiments expressed the luciferase gene; therefore, tumor growth was measured weekly by injecting luciferin (Thermo Fisher Scientific), waiting for 7 min, and imaging isoflurane- anaesthetized mice with the IVIS Spectrum Bioimager (PerkinElmer).

**High-parameter flow cytometry LEGENDScreen and Infinity Flow**

Infinity Flow was conducted as previously described (*24*); cells from mice treated with tamoxifen at days 14/15, 21/22, and 28/29 were labeled with a specific anti- CD45 barcoding antibody: CD45-BUV395, CD45-BUV661, and CD45- APC- Cy7. Barcoded cells were pooled and incubated with a "backbone" flow cytometry panel including antibodies recognizing markers that discriminated monocytes, macrophages, and neutrophils. The antibodies used for the backbone were specific for Ly6G (1A8), Siglec-F (E50- 2440), CD101 (Moushi101), Gr- 1 (RB6- 8C5), Ly6C (HK1.4), CD11b (M1/70), I- A/I- E (M5/114.15.2), B220 (53- 6.7), CD90.2 (53- 2.1), NK1.1 (PK136), CD11c (N418), CD45 (30- F11), and CD43 (S7). Labeled and barcoded cells were placed into a 96-well U- bottom plate, and a unique phycoerythrin (PE)– conjugated antibody was added to each well, as per the LEGENDScreen kit (BioLegend). Fully labeled cells were acquired on a 5-laser LSR II (BD Biosciences) using Diva software (BD Biosciences). Each subsequent .fcs file with a unique PE- conjugated antibody and the backbone was analyzed using FlowJo (BD Biosciences). Marker expression across cell types was predicted using the learning algorithm XGBoost implemented in Infinity Flow pipeline as previously described (*24*). Briefly, input data were subjected to logicle transformation, calculating a $z$- score for all backbone markers, before implementing the XGBoost R package, which trains a multivariate regression model and imputes the intensity expression of each marker on each cell into one concatenated .fcs file. The generated .fcs file is then used for downstream analysis. All downstream analysis was performed using FlowJo (BD Biosciences) and the R package Seurat (*55*). Dimensional reduction [principal components analysis (PCA) and UMAP] and clustering were performed using nearest- neighbor analysis by the Seurat package. Statistical analysis was performed by identifying differentially expressed proteins using a Wilcoxon rank sum test. $P$ values of $<0.05$ were considered statistically significant.

**Single- cell RNA sequencing**

tdTomato$^{+/-}$ cell populations were sorted from *Ms4a3*$^{Cre}$ *x Rosa*$^{tdTomato}$ and *Ms4a3*$^{CreERT2}$ x *Rosa*$^{tdTomato}$ mice using the indicated gating strategies. The cells were processed using the Chromium Single Cell 3′ (v3 Chemistry) platform (10x Genomics). tdTomato$^{+}$ and tdTomato$^{-}$ cells were sequenced separately using the NovaSeq sequencer (Illumina). Briefly, cells were loaded onto a Chromium Next GEM Chip G, and single- cell suspensions in gel beads-in- emulsion (GEMs) were generated using the chromium controller (10x Genomics). Reverse transcription was performed to generate cDNA, which was amplified, cleaned, and fragmented. Last, libraries were subjected to standard quality control (QC) steps before sequencing.

*Published in : Science Immunology (2024), vol. 9, eadk3981*
*DOI: 10.1126/sciimmunol.adk3981*
*Status : Postprint (Author's version)*

**Analysis of scRNA- seq data**

Raw counts were aligned to the GRCm38 mm10 *Mus musculus* genome from the Genome Reference Consortium using STAR 2.5.3a (*56*). Counts were log- normalized and scaled, and dimensionality reduction was performed (PCA and UMAP). Nearest- neighbor analysis was used for stable clustering. A bimodal likelihood ratio test was performed, comparing each cluster with all other clusters to identify DEGs with an adjusted $P$ value of $<0.05$ and a log fold change (logFC) of $\geq 0.25$ (*57*). To integrate cells from different human PDAC datasets, we applied 10 rounds of clustering and correction steps using Harmony with parameters "epsilon.harmony = - Inf, max.iter.harmony =10." To cluster single cells by their expression profiles, we used the functions FindNeighbors and FindClusters with an appropriate number of Harmony reduction (10 to 15) and resolution (0.6 to 0.8) to perform unsupervised graph–based clustering. To compare monocytes and TAMs from human PDAC and murine PDAC, we used SciBet (version 0.1.0) (*58*), a supervised cell- type identifier based on $E$ test to predict cell identities for mouse PDAC using cells from human PDAC as references. The SelectGene function in SciBet selected the marker genes for each subset. Pseudotime and trajectory analysis were performed using the R packages Slingshot (*22*), scVelo (*21*), and PAGA (*40*). Transcription factor activity prediction was performed using SCENIC (*28*). GO analysis was performed by uploading DEGs from scRNA- seq analysis to Metascape (*29*). Interactome analysis was performed using CellChat (*30*) and RNA Magnet (*31*). Alluvial plots were made using ggplot2, and circus plots were made using the circlize package in R (*59*).

**10x Visium spatial transcriptomics**

The 10x data presented here were previously published as GSE244534 (*32*); however, the analysis of the data was performed independently. Two tumor tissue sections were collected at day 14 (shown as top two panels in fig. S10A), and two were collected at day 42 (shown as panel in Fig. 5B and top panel in S10A) and were fixed and frozen using the specifications listed by 10x recommendations. Tissue sections were made by cutting frozen tissues with a cryostat (CM3050S, Leica) at 10-μ m thickness and mounted on Visium slides (10x Genomics). RNA was extracted following the 10x protocol. QC was performed using the RNA 6000 Pico kit (Agilent). Sequenced reads were aligned in Cell Ranger software (10x Genomics) using the mm10 genome and underwent standard QC. The output was then analyzed further as a single- cell object using the BayesSpace R package (*33*). Briefly, spatial clusters were assigned using the mclust function, and spot enhancement was performed. Cell- type signatures were selected using the top 10 DEGs (adjusted $P$ value of $<0.05$ and a logFC of $\geq 0.25$) identified by scRNA-seq scored by a sum of the log counts and then projected onto the spatial transcriptomics data.

**CODEX multiplex imaging and analysis**

Slices (5 μm) of embedded murine PDAC (day 35 after orthotopic injection) were prepared and used for CODEX labeling following the manufacturer's instructions. Briefly, sections were retrieved from the freezer, rehydrated, and photobleached as described in (*60*). After photobleaching, sections were blocked and incubated with a 21-plex CODEX antibody panel overnight at 4°C. After washing, samples were fixed with ice-cold methanol, washed again with PBS, and fixed for 20 min with bis sulfosuccinimidyl suberate (BS3) fixative (Thermo Fisher Scientific). Samples were subsequently

*Published in : Science Immunology (2024), vol. 9, eadk3981*
*DOI: 10.1126/sciimmunol.adk3981*
*Status : Postprint (Author's version)*

washed with PBS and stored at 4°C for a maximum of 1 week before imaging. Sections were equilibrated at room temperature before imaging. Antibody detection was performed in a multicycle experiment, following the manufacturer's instructions. Images were acquired with a Zeiss Axio Observer widefield fluorescence microscope using a 40× objective (numerical aperture, 0.85) and $z$-spacing of 1.5 μm. The 405- , 488- , 568- , and 647- nm channels were used for acquisition. Images were exported using the CODEX Instrument Manager (Akoya Biosciences) and processed with CODEX Processor v1.7 (Akoya Biosciences). Processing steps included background subtraction, deconvolution, shading correction, stitching, and cell segmentation. 4′,6- Diamidino- 2- phenylindole counterstain was used for object detection, whereas sodium potassium adenosine triphosphatase antibody labeling was used to mark membranes for delineating cell shape. Our defined gating strategy identified imaged cells as distinct cell types (monocytes, IntTAMs, TAM2, and TAM3). Cell types were projected onto the tissue section, and distance from hypoxic/necrotic tissue was calculated for each cell type. To define cell- to-cell interactions, we identified cell types as monocytes, IntTAMs, TAM2s, or TAM3s. We also defined other cell types using common cell markers. A raster scan algorithm using a radius of 50 μm was used. The objects generated were subsequently clustered on the basis of the cellular local composition defining tissue regions or cellular neighborhoods. Next, we looked at cells surrounding monocytes, IntTAMs, TAM2s, or TAM3s within the regions, in which these populations were predominant. We then calculated an interaction score on the basis of the frequency of these cell types interacting. These scores were validated in the images.

**Survival and treatment response data**

The Cox proportional hazards model implemented in the R package survival was used to perform survival analyses. The R function ggsurvplot was used to plot Kaplan- Meier survival curves using data from 178 patients with primary pancreatic adenocarcinomas from TCGA, which were used to evaluate the impact of Hu.TAM a to e signatures on overall survival. Differences in age and gender were corrected for in the Cox model. Response to treatment was measured as described ($35$). Briefly, population variability was normalized using a Dirichlet-multinomial regression, and stats were calculated us- ing a nonparametric Mann- Whitney $U$ test.

**Statistical analysis**

All statistical analyses were performed with Prism 5.0 (GraphPad Software). All $P$ values are two tailed. Other statistical analysis was performed using R as described in detail for each dataset, depending on the approach.

*Published in : Science Immunology (2024), vol. 9, eadk3981*
*DOI: 10.1126/sciimmunol.adk3981*
*Status : Postprint (Author's version)*

Supplementary Materials

**The PDF file includes**:

Materials and methods

Figs. S1 to S13

Tables S1 and S2

References (*61–63*)

**Other Supplementary Material for this manuscript includes the following**:

Data files S1 to S11

MDaR Reproducibility checklist

# REFERENCES AND NOTES

1. Y . Iwai, M. Ishida, Y. Tanaka, T. Okazaki, T. Honjo, N. Minato, Involvement of PD-L1 on tumor cells in the escape from host immune system and tumor immunotherapy by PD-L1 blockade. Proc. Natl. Acad. Sci. U.S.A. 99, 12293–12297 (2002).

2. D. R. Leach, M. F. Krummel, J. P. Allison, Enhancement of antitumor immunity by CTLA -4 blockade. Science 271, 1734–1736 (1996).

3. C . Robert, G. V. Long, B. Brady, C. Dutriaux, M. Maio, L. Mortier, J. C. Hassel, P. Rutkowski, C. McNeil, E. Kalinka-Warzocha, K. J. Savage, M. M. Hernberg, C. Lebbé, J. Charles, C. Mihalcioiu, V. Chiarion-Sileni,

C. Mauch, F. Cognetti, A. Arance, H. Schmidt, D. Schadendorf, H. Gogas, L. Lundgren-Eriksson, C. Horak, B. Sharkey, I. M. Waxman, V. Atkinson, P. A. Ascierto, Nivolumab in previously untreated melanoma without BRAF mutation. N. Engl. J. Med. 372, 320–330 (2015).

4. J. Bian, K. Almhanna, Pancreatic cancer and immune checkpoint inhibitors—still a long way to go. Transl. Gastroenterol. Hepatol. 6, 6 (2021).

5. M . D. Park, A. Silvin, F. Ginhoux, M. Merad, Macrophages in health and disease. Cell 185, 4259–4279 (2022).

6. A . Mantovani, F. Marchesi, A. Malesci, L. Laghi, P. Allavena, Tumour-associated macrophages as treatment targets in oncology. Nat. Rev. Clin. Oncol. 14, 399–416 (2017).

7. K. Mulder, A. A. Patel, W. T. Kong, C. Piot, E. Halitzki, G. Dunsmore, S. Khalilnezhad, S. E. Irac, A. Dubuisson, M. Chevrier, X. M. Zhang, J. K. C. Tam, T. K. H. Lim, R. M. M. Wong, R. Pai, A. I. S. Khalil, P. K. H. Chow, S. Z. Wu, G. al-Eryani, D. Roden, A. Swarbrick, J. K. Y. Chan, S. Albani, L. Derosa, L. Zitvogel, A. Sharma, J. Chen, A. Silvin, A. Bertoletti, C. Blériot, C. A. Dutertre, F. Ginhoux, Cross-tissue

single-cell landscape of human monocytes and macrophages in health and disease. Immunity 54, 1883–1900.e5 (2021).

8. S. Cheng, Z. Li, R. Gao, B. Xing, Y. Gao, Y. Yang, S. Qin, L. Zhang, H. Ouyang, P. du, L. Jiang, B. Zhang, Y. Yang, X. Wang, X. Ren, J. X. Bei, X. Hu, Z. Bu, J. Ji, Z. Zhang, A pan-cancer single-cell transcriptional atlas of tumor infiltrating myeloid cells. Cell 184, 792–809.e23 (2021).

9. C . Bleriot, S. Chakarov, F. Ginhoux, Determinants of resident tissue macrophage identity and function. Immunity 52, 957–970 (2020).

10. F. Ginhoux, M. Guilliams, Tissue-resident macrophage ontogeny and homeostasis. Immunity 44, 439–449 (2016).

11. Y . Zhu, J. M. Herndon, D. K. Sojka, K. W. Kim, B. L. Knolhoff, C. Zuo, D. R. Cullinan, J. Luo, A. R. Bearden, K. J. Lavine, W. M. Yokoyama, W. G. Hawkins, R. C. Fields, G. J. Randolph, D. G. DeNardo, Tissue-resident macrophages in pancreatic ductal adenocarcinoma originate from embryonic hematopoiesis and promote tumor progression. Immunity 47, 323–338.e6 (2017).

12. M . Casanova-Acebes, E. Dalla, A. M. Leader, J. LeBerichel, J. Nikolic, B. M. Morales, M. Brown, C. Chang, L. Troncoso, S. T. Chen, A. Sastre-Perona, M. D. Park, A. Tabachnikova, M. Dhainaut, P. Hamon, B. Maier, C. M. Sawai, E. Agulló-Pascual, M. Schober, B. D. Brown, B. Reizis, T. Marron, E. Kenigsberg, C. Moussion, P. Benaroch, J. A. Aguirre-Ghiso, M. Merad, Tissue-resident macrophages provide a pro-tumorigenic niche to early NSCLC cells. Nature 595, 578–584 (2021).

13. Z. Liu, Y. Gu, S. Chakarov, C. Bleriot, I. Kwok, X. Chen, A. Shin, W. Huang, R. J. Dress, C. A. Dutertre, A. Schlitzer, J. Chen, L. G. Ng, H. Wang, Z. Liu, B. Su, F. Ginhoux, Fate mapping via Ms4a3-expression history traces monocyte-derived cells. Cell 178, 1509–1525.e19 (2019).

14. R. Nalio Ramos, Y. Missolo-Koussou, Y. Gerber-Ferder, C. P. Bromley, M. Bugatti, N. G. Núñez, J. Tosello Boari, W. Richer, L. Menger, J. Denizeau, C. Sedlik, P. Caudana, F. Kotsias, L. L. Niborski, S. Viel, M. Bohec, S. Lameiras, S. Baulande, L. Lesage, A. Nicolas, D. Meseure, A. Vincent-Salomon, F. Reyal, C. A. Dutertre, F. Ginhoux, L. Vimeux, E. Donnadieu, B. Buttard, J. Galon, S. Zelenay, W. Vermi, P. Guermonprez, E. Piaggio, J. Helft, Tissue-resident FOLR2$^+$ macrophages associate with CD8$^+$ T cell infiltration in human breast cancer. Cell 185, 1189–1207.e25 (2022).

15. A . Chow, S. Schad, M. D. Green, M. D. Hellmann, V. Allaj, N. Ceglia, G. Zago, N. S. Shah, S. K. Sharma, M. Mattar, J. Chan, H. Rizvi, H. Zhong, C. Liu, Y. Bykov, D. Zamarin, H. Shi, S. Budhu, C. Wohlhieter, F. Uddin, A. Gupta, I. Khodos, J. J. Waninger, A. Qin, G. J. Markowitz, V. Mittal, V. Balachandran, J. N. Durham, D. T. le, W. Zou, S. P. Shah, A. McPherson, K. Panageas, J. S. Lewis, J. S. A. Perry, E. de Stanchina, T. Sen, J. T. Poirier, J. D. Wolchok, C. M. Rudin, T. Merghoub, Tim-4$^+$ cavity-resident macrophages impair anti-tumor CD8$^+$ T cell immunity. Cancer Cell 39, 973–988.e9 (2021).

16. R. E. Menjivar, Z. C. Nwosu, W. du, K. L. Donahue, H. S. Hong, C. Espinoza, K. Brown,,A. Velez-Delgado, W. Yan, F. Lima, A. Bischoff, P. Kadiyala, D. Salas-Escabillas, H. C. Crawford, F. Bednar, E. Carpenter, Y. Zhang, C. J. Halbrook, C. A. Lyssiotis, M. Pasca di Magliano, Arginase 1 is a key driver of immune suppression in pancreatic cancer. eLife 12, e80721 (2023).

17. L . Zhang, Z. Li, K. M. Skrzypczynska, Q. Fang, W. Zhang, S. A. O'Brien, Y. He, L. Wang, Q. Zhang, A. Kim, R. Gao, J. Orf, T. Wang, D. Sawant, J. Kang, D. Bhatt, D. Lu, C. M. Li, A. S. Rapaport, K. Perez, Y. Ye, S. Wang, X. Hu, X. Ren, W. Ouyang, Z. Shen, J. G. Egen, Z. Zhang, X. Yu, Single-cell analyses inform mechanisms of myeloid-targeted therapies in colon cancer. Cell 181, 442–459.e29 (2020).

18. E . Kerkelä, R. Ala-aho, P. Klemi, S. Grénman, S. D. Shapiro, V.-M. Kähäri, U. Saarialho-Kere, Metalloelastase (MMP-12) expression by tumour cells in squamous cell carcinoma of the vulva correlates with invasiveness, while that by macrophages predicts better outcome. J. Pathol. 198, 258–269 (2002).

19. E . Timperi, P. Gueguen, M. Molgora, I. Magagna, Y. Kieffer, S. Lopez-Lastra, P. Sirven, L. G. Baudrin, S. Baulande, A. Nicolas, G. Champenois, D. Meseure, A. Vincent-Salomon, A. Tardivon, E. Laas, V. Soumelis, M. Colonna, F. Mechta-Grigoriou, S. Amigorena, E. Romano, Lipid-associated macrophages are induced by cancer-associated fibroblasts and mediate immune suppression in breast cancer. Cancer Res. 82, 3291–3306 (2022).

20. D. A. Jaitin, L. Adlung, C. A. Thaiss, A. Weiner, B. Li, H. Descamps, P. Lundgren, C. Bleriot, Z. Liu, A. Deczkowska, H. Keren-Shaul, E. David, N. Zmora, S. M. Eldar, N. Lubezky, O. Shibolet, D. A. Hill, M. A. Lazar, M. Colonna, F. Ginhoux, H. Shapiro, E. Elinav, I. Amit, Lipid-associated macrophages control metabolic homeostasis in a Trem2-dependent manner. Cell 178, 686–698.e14 (2019).

21. V. Bergen, M. Lange, S. Peidli, F. A. Wolf, F. J. Theis, Generalizing RNA velocity to transient cell states through dynamical modeling. Nat. Biotechnol. 38, 1408–1414 (2020).

22. K. Street, D. Risso, R. B. Fletcher, D. das, J. Ngai, N. Yosef, E. Purdom, S. Dudoit, Slingshot: Cell lineage and pseudotime inference for single-cell transcriptomics. BMC Genomics 19, 477 (2018).

23. E . Becht, D. Tolstrup, C. A. Dutertre, P. A. Morawski, D. J. Campbell, F. Ginhoux, E. W. Newell, R. Gottardo, M. B. Headley, High-throughput single-cell quantification of hundreds of proteins using conventional flow cytometry and machine learning. Sci. Adv. 7, eabg0505 (2021).

24. C . A. Dutertre, E. Becht, S. E. Irac, A. Khalilnezhad, V. Narang, S. Khalilnezhad, P. Y. Ng, L. L. van den Hoogen, J. Y. Leong, B. Lee, M. Chevrier, X. M. Zhang, P. J. A. Yong, G. Koh, J. Lum, S. W. Howland, E. Mok, J. Chen, A. Larbi, H. K. K. Tan, T. K. H. Lim, P. Karagianni, A. G. Tzioufas, B. Malleret, J. Brody, S. Albani, J. van Roon, T. Radstake, E. W. Newell, F. Ginhoux, Single-cell analysis of human mononuclear phagocytes reveals subset-defining markers and identifies circulating inflammatory dendritic cells. Immunity 51, 573–589.e8 (2019).

25. M . D. Park, I. Reyes-Torres, J. LeBerichel, P. Hamon, N. M. LaMarche, S. Hegde, M. Belabed, L. Troncoso, J. A. Grout, A. Magen, E. Humblin, A. Nair, M. Molgora, J. Hou, J. H. Newman, A. M. Farkas, A. M. Leader, T. Dawson, D. D'Souza, S. Hamel, A. R. Sanchez-Paulete, B. Maier, N. Bhardwaj, J. C. Martin, A. O. Kamphorst, E. Kenigsberg, M. Casanova-Acebes, A. Horowitz, B. D. Brown, L. F. de Andrade, M. Colonna, T. U. Marron, M. Merad, TREM2 macrophages drive NK cell paucity and dysfunction in lung cancer. Nat. Immunol. 24, 792–801 (2023).

26. M . Molgora, E. Esaulova, W. Vermi, J. Hou, Y. Chen, J. Luo, S. Brioschi, M. Bugatti, A. S. Omodei, B. Ricci, C. Fronick, S. K. Panda, Y. Takeuchi, M. M. Gubin, R. Faccio, M. Cella, S. Gilfillan, E. R. Unanue, M. N. Artyomov, R. D. Schreiber, M. Colonna, TREM2 modulation remodels the tumor myeloid landscape enhancing anti-PD-1 immunotherapy. Cell 182, 886–900.e17 (2020).

27. H . Keren-Shaul, A. Spinrad, A. Weiner, O. Matcovitch-Natan, R. Dvir-Szternfeld, T. K. Ulland, E. David, K. Baruch, D. Lara-Astaiso, B. Toth, S. Itzkovitz, M. Colonna, M. Schwartz, I. Amit, Aunique microglia type associated with restricting development of Alzheimer's disease. Cell 169, 1276–1290.e17 (2017).

28. S. Aibar, C. B. González-Blas, T. Moerman, V. A. Huynh-Thu, H. Imrichova, G. Hulselmans, F. Rambow, J. C. Marine, P. Geurts, J. Aerts, J. van den Oord, Z. K. Atak, J. Wouters, S. Aerts, SCENIC: Single-cell regulatory network inference and clustering. Nat. Methods 14, 1083–1086 (2017).

29. Y . Zhou, B. Zhou, L. Pache, M. Chang, A. H. Khodabakhshi, O. Tanaseichuk, C. Benner, S. K. Chanda, Metascape provides a biologist-oriented resource for the analysis of systems-level datasets. Nat. Commun. 10, 1523 (2019).

30. S. Jin, C. F. Guerrero-Juarez, L. Zhang, I. Chang, R. Ramos, C. H. Kuan, P. Myung, M. V. Plikus, Q. Nie, Inference and analysis of cell-cell communication using CellChat. Nat. Commun. 12, 1088 (2021).

31. C . Baccin, J. al-Sabah, L. Velten, P. M. Helbling, F. Grünschl.ger, P. Hernández-Malmierca, C. Nombela-Arrieta, L. M. Steinmetz, A. Trumpp, S. Haas, Combined single-cell and spatial transcriptomics reveal the molecular, cellular and spatial bone marrow niche organization. Nat. Cell Biol. 22, 38–48 (2020).

32. M . S. F. Ng, I. Kwok, L. Tan, C. Shi, D. Cerezo-Wallis, Y. Tan, K. Leong, G. F. Calvo, K. Yang, Y. Zhang, J. Jin, K. H. Liong, D. Wu, R. He, D. Liu, Y. C. Teh, C. Bleriot, N. Caronni, Z. Liu, K. Duan, V. Narang, I. Ballesteros, F. Moalli, M. Li, J. Chen, Y. Liu, L. Liu, J. Qi, Y. Liu, L. Jiang, B. Shen, H. Cheng, T. Cheng, V. Angeli, A. Sharma, Y. H. Loh, H. L. Tey, S. Z. Chong, M. Iannacone, R. Ostuni, A. Hidalgo, F. Ginhoux, L. G. Ng, Deterministic reprogramming of neutrophils within tumors. Science 383, eadf6493 (2024).

33. E . Zhao, M. R. Stone, X. Ren, J. Guenthoer, K. S. Smythe, T. Pulliam, S. R. Williams, C. R. Uytingco, S. E. B. Taylor, P. Nghiem, J. H. Bielas, R. Gottardo, Spatial transcriptomics at subspot resolution with BayesSpace. Nat. Biotechnol. 39, 1375–1384 (2021).

34. Y . Goltsev, N. Samusik, J. Kennedy-Darling, S. Bhate, M. Hale, G. Vazquez, S. Black, G. P. Nolan, Deep profiling of mouse splenic architecture with CO DEX multiplexed imaging. Cell 174, 968–981.e15 (2018).

35. W. L. Hwang, K. A. Jagadeesh, J. A. Guo, H. I. Hoffman, P. Yadollahpour, J. W. Reeves, R. Mohan, E. Drokhlyansky, N. van Wittenberghe, O. Ashenberg, S. L. Farhi, D. Schapiro, P. Divakar, E. Miller, D. R. Zollinger, G. Eng, J. M. Schenkel, J. Su, C. Shiau, P. Yu, W. A. Freed-Pastor, D. Abbondanza, A. Mehta, J. Gould, C. Lambden, C. B. M. Porter, A. Tsankov, D. Dionne, J. Waldman, M. S. Cuoco, L. Nguyen, T. Delorey, D. Phillips, J. L. Barth, M. Kem, C. Rodrigues, D. Ciprani, J. Roldan, P. Zelga, V. Jorgji, J. H. Chen, Z. Ely, D. Zhao, K. Fuhrman, R. Fropf, J. M. Beechem, J. S. Loeffler, D. P. Ryan, C. D.

Weekes, C. R. Ferrone, M. Qadan, M. J. Aryee, R. K. Jain, D. S. Neuberg, J. Y. Wo, T. S. Hong, R. Xavier, A. J. Aguirre, O. Rozenblatt-Rosen, M. Mino-Kenudson, C. F. D. Castillo, A. S. Liss, D. T. Ting, T. Jacks, A. Regev, Single-nucleus and spatial transcriptome profiling of pancreatic cancer identifies multicellular dynamics associated with neoadjuvant treatment. Nat. Genet. 54, 1178–1191 (2022).

36. K. Chen, Y. Wang, Y. Hou, Q. Wang, D. Long, X. Liu, X. Tian, Y. Yang, Single cell RNA-seq reveals the CCL 5/SDC1 receptor-ligand interaction between T cells and tumor cells in pancreatic cancer. Cancer Lett. 545, 215834 (2022).

37. N . G. Steele, E. S. Carpenter, S. B. Kemp, V. R. Sirihorachai, S. The, L. Delrosario, J. Lazarus, E. A. D. Amir, V. Gunchick, C. Espinoza, S. Bell, L. Harris, F. Lima, V. Irizarry-Negron, D. Paglia, J. Macchia, A. K. Y. Chu, H. Schofield, E. J. Wamsteker, R. Kwon, A. Schulman, A. Prabhu, R. Law, A. Sondhi, J. Yu, A. Patel, K. Donahue, H. Nathan, C. Cho, M. A. Anderson, V. Sahai, C. A. Lyssiotis, W. Zou, B. L. Allen, A. Rao, H. C. Crawford, F. Bednar, T. L. Frankel, M. Pasca di Magliano, Multimodal mapping of the tumor and peripheral blood immune landscape in human pancreatic cancer. Nat. Cancer 1, 1097–1112 (2020).

38. J. Peng, B. F. Sun, C. Y. Chen, J. Y. Zhou, Y. S. Chen, H. Chen, L. Liu, D. Huang, J. Jiang, G. S. Cui, Y. Yang, W. Wang, D. Guo, M. Dai, J. Guo, T. Zhang, Q. Liao, Y. Liu, Y. L. Zhao, D. L. Han, Y. Zhao, Y. G. Yang, W. Wu, Single-cell RNA-seq highlights intra-tumoral heterogeneity and malignant progression in pancreatic ductal adenocarcinoma. Cell Res. 29, 725–738 (2019).

39. T . Stuart, A. Butler, P. Hoffman, C. Hafemeister, E. Papalexi, W. M. Mauck III, Y. Hao, M. Stoeckius, P. Smibert, R. Satija, Comprehensive integration of single-cell data. Cell 177, 1888–1902.e21 (2019).

40. F. A. Wolf, F. K. Hamey, M. Plass, J. Solana, J. S. Dahlin, B. Göttgens, N. Rajewsky, L. Simon, F. J. Theis, PAGA : Graph abstraction reconciles clustering with trajectory inference through a topology preserving map of single cells. Genome Biol. 20, 59 (2019).

41. J. Villar, L. Ouaknin, A. Cros, E. Segura, Monocytes differentiate along two alternative pathways during sterile inflammation. EMBO Rep. 24, e56308 (2023).

42. A. Subramanian, P. Tamayo, V. K. Mootha, S. Mukherjee, B. L. Ebert, M. A. Gillette, A. Paulovich, S. L. Pomeroy, T. R. Golub, E. S. Lander, J. P. Mesirov, Gene set enrichment analysis: A knowledge-based approach for interpreting genome-wide expression profiles. Proc. Natl. Acad. Sci. U.S.A. 102, 15545–15550 (2005).

43. V. K. Mootha, C. M. Lindgren, K. F. Eriksson, A. Subramanian, S. Sihag, J. Lehar, P. Puigserver, E. Carlsson, M. Ridderstråle, E. Laurila, N. Houstis, M. J. Daly, N. Patterson, J. P. Mesirov, T. R. Golub, P. Tamayo, B. Spiegelman, E. S. Lander, J. N. Hirschhorn, D. Altshuler, L. C. Groop, PGC-1α-responsive genes involved in oxidative phosphorylation are coordinately downregulated in human diabetes. Nat. Genet. 34, 267–273 (2003).

44. The Cancer Genome Atlas Program (TCGA) (National Cancer Institute's Center for Cancer Genomics, 2023); www.cancer.gov/ccg/research/genome-sequencing/tcga.

45. V. Mysore, S. Tahir, K. Furuhashi, J. Arora, F. Rosetti, X. Cullere, P. Yazbeck, M. Sekulic, M. E. Lemieux, S. Raychaudhuri, B. H. Horwitz, T. N. Mayadas, Monocytes transition to macrophages within the inflamed vasculature via monocyte CCR2 and endothelial TNFR2. J. Exp. Med. 219, e20210562 (2022).

46. Y. Katzenelenbogen, F. Sheban, A. Yalin, I. Yofe, D. Svetlichnyy, D. A. Jaitin, C. Bornstein, A. Moshe, H. Keren-Shaul, M. Cohen, S. Y. Wang, B. Li, E. David, T. M. Salame, A. Weiner, I. Amit, Coupled scRNA-seq and intracellular protein activity reveal an immunosuppressive role of TREM2 in cancer. Cell 182, 872–885.e19 (2020).

47. A. T. Henze, M. Mazzone, The impact of hypoxia on tumor-associated macrophages. J. Clin. Invest. 126, 3672–3679 (2016).

48. R. Bill, P. Wirapati, M. Messemaker, W. Roh, B. Zitti, F. Duval, M. Kiss, J. C. Park, T. M. Saal, J. Hoelzl, D. Tarussio, F. Benedetti, S. Tissot, L. Kandalaft, M. Varrone, G. Ciriello, T. A. McKee, Y. Monnier, M. Mermod, E. M. Blaum, I. Gushterova, A. L. K. Gonye, N. Hacohen, G. Getz, T. R. Mempel, A. M. Klein, R. Weissleder, W. C. Faquin, P. M. Sadow, D. Lin, S. I. Pai, M. Sade-Feldman, M. J. Pittet, CXCL9:SPP1 macrophage polarity identifies a network of cellular programs that control human cancers. Science 381, 515–524 (2023).

49. A. Sebestyen, L. Kopper, T. Danko, J. Timar, Hypoxia signaling in cancer: From basics to clinical practice. Pathol. Oncol. Res. 27, 1609802 (2021).

50. C. Bleriot, G. Dunsmore, D. Alonso--Curbelo, F. Ginhoux, A temporal perspective for tumor associated macrophage identities and functions. Cancer Cell 42, 747–758 (2024).

51. C. Bleriot, T. Dupuis, G. Jouvion, G. Eberl, O. Disson, M. Lecuit, Liver-resident macrophage necroptosis orchestrates type 1 microbicidal inflammation and type-2-mediated tissue repair during bacterial infection. Immunity 42, 145–158 (2015).

52. D. Vanneste, Q. Bai, S. Hasan, W. Peng, D. Pirottin, J. Schyns, P. Maréchal, C. Ruscitti, M. Meunier, Z. Liu, C. Legrand, L. Fievez, F. Ginhoux, C. Radermecker, F. Bureau, T. Marichal, MafB-restricted local monocyte proliferation precedes lung interstitial macrophage differentiation. Nat. Immunol. 24, 827–840 (2023).

53. H. L. Penny, J. L. Sieow, S. Y. Gun, M. C. Lau, B. Lee, J. Tan, C. Phua, F. Toh, Y. Nga, W. H. Yeap, B. Janela, D. Kumar, H. Chen, J. Yeong, J. A. Kenkel, A. Pang, D. Lim, H. C. Toh, T. L. K. Hon, C. I. Johnson, H. J. Khameneh, A. Mortellaro, E. G. Engleman, O. Rotzschke, F. Ginhoux, J. P. Abastado, J. Chen, S. C. Wong, Targeting glycolysis in macrophages confers protection against pancreatic ductal adenocarcinoma. Int. J. Mol. Sci. 22, 6350 (2021).

54. N. M. Aiello, A. D. Rhim, B. Z. Stanger, Orthotopic injection of pancreatic cancer cells. Cold Spring Harb. Protoc. 2016, pdb.prot078360 (2016).
55. Y. Hao, S. Hao, E. Andersen--Nissen, W. M. Mauck III, S. Zheng, A. Butler, M. J. Lee, A. J. Wilk, C. Darby, M. Zager, P. Hoffman, M. Stoeckius, E. Papalexi, E. P. Mimitou, J. Jain, A. Srivastava, T. Stuart, L. M. Fleming, B. Yeung, A. J. Rogers, J. M. McElrath, C. A. Blish, R. Gottardo, P. Smibert, R. Satija, Integrated analysis of multimodal single-cell data. Cell 184, 3573–3587.e29 (2021).
56. A. Dobin, C. A. Davis, F. Schlesinger, J. Drenkow, C. Zaleski, S. Jha, P. Batut, M. Chaisson, T. R. Gingeras, STAR: Ultrafast universal RNA-seq aligner. Bioinformatics 29, 15–21 (2013).
57. A. McDavid, G. Finak, P. K. Chattopadyay, M. Dominguez, L. Lamoreaux, S. S. Ma, M. Roederer, R. Gottardo, Data exploration, quality control and testing in single-cell qPCR-based gene expression experiments. Bioinformatics 29, 461–467 (2013).
58. C. Li, B. Liu, B. Kang, Z. Liu, Y. Liu, C. Chen, X. Ren, Z. Zhang, SciBet as a portable and fast single cell type identifier. Nat. Commun. 11, 1818 (2020).
59. Z. Gu, L. Gu, R. Eils, M. Schlesner, B. Brors, circlize implements and enhances circular visualization in R. Bioinformatics 30, 2811–2812 (2014).
60. Z. Du, J.-R. Lin, R. Rashid, Z. Maliga, S. Wang, J. C. Aster, B. Izar, P. K. Sorger, S. Santagata, Qualifying antibodies for image-based immune profiling and multiplexed tissue imaging. Nat. Protoc. 14, 2900–2930 (2019).
61. S. Hanzelmann, R. Castelo, J. Guinney, GSVA: Gene set variation analysis for microarray and RNA-seq data. BMC Bioinformatics 14, 7 (2013).
62. P. Bankhead, M. B. Loughrey, J. A. Fernández, Y. Dombrowski, D. G. McArt, P. D. Dunne, S. McQuaid, R. T. Gray, L. J. Murray, H. G. Coleman, J. A. James, M. Salto--Tellez, P. W. Hamilton, QuPath: Open source software for digital pathology image analysis. Sci. Rep. 7, 16878 (2017).
63. J. Schindelin, I. Arganda--Carreras, E. Frise, V. Kaynig, M. Longair, T. Pietzsch, S. Preibisch, C. Rueden, S. Saalfeld, B. Schmid, J. Y. Tinevez, D. J. White, V. Hartenstein, K. Eliceiri, P. Tomancak, A. Cardona, Fiji: An open-source platform for biological-image analysis. Nat. Methods 9, 676–682 (2012).

*Published in : Science Immunology (2024), vol. 9, eadk3981*
*DOI: 10.1126/sciimmunol.adk3981*
*Status : Postprint (Author's version)*

**Acknowledgments:** We thank the W. S. Cheng laboratory for the use of the KPC pancreatic cancer model described here. We thank M. Lecuit laboratory for providing the Ccr2-KO mice. We thank the animal facilities in the Institute Gustave Roussy, Shanghai Jiao Tong University School of Medicine, and Singapore Immunology Network for ensuring that all protocols were performed within the appropriate ethical considerations. We thank the members of U1015 for helpful discussion. We thank L. Robinson for the invaluable input and editing of this manuscript. **Funding**: We thank the ARC Foundation (Recruiting International Leaders 2020) and Fondation Gustave Roussy for the financial support in this work. A.S. and D.A.B. were funded by the Deutsche Forschungsgemeinschaft (DFG; German Research Foundation) under Germany's Excellence Strategy–EXC2151–390873048 (A.S. and D.A.B.) and the SFB 1454-P05-432325352 (A.S. and D.A.B.). **Author contributions**: G.D., W.G., D.A.B., K.Y., L.T., M.N., I.K., A.B., M.B., R.P., A.Y., C.D.L.C.F., Z.L., S.C., and C.B. performed experimentation. G.D., Z.L., D.A.B., I.K., B.K., A.B., A.Y., J.T., J.V., K.M., and C.B. performed formal analysis. Z.L., J.-Y.S., and G.G. performed data curation. C.-A.D., S.C., Z.L., A.-M.L.-D., B.S., C.S.-F., W.H.F., A. Sharma, and A. Schlitzer provided invaluable advice. L.G.N., C.B., and F.G. supervised the project. C.B. and F.G. acquired funding for the project. G.D., C.B., and F.G. wrote the original draft of the paper. **Competing interests**: F.G. and C.B. are inventors on patent application (PCT /EP2024/060644) submitted by Gustave Roussy Hospital that covers detecting TAM s in pancreatic cancer. The other authors declare that they have no competing interests. **Data and materials availability**: All data needed to evaluate the conclusions in the paper are present in the paper or the Supplementary Materials. All generated scRNA-seqdata have been deposited in the NCBI Gene Expression Omnibus under accession number GSE270793. Tabulated data underlying the main figures are provided in data file S11. Mouse models (Ms4a3$^{Cre}$, Ms4a3$^{CreERT2}$, and Trem2$^{EGFP}$) are available upon request to F.G. after execution of a material transfer agreement with the Shanghai Institute of Immunology.